UCSF

Title

mTOR inhibition reprograms cellular proteostasis by regulating eIF3D-mediated selective mRNA translation and promotes cell phenotype switching.

Permalink

https://escholarship.org/uc/item/7pf1r583

Journal

Authors

Shin, Sejeong
Han, Min-Joon
Jedrychowski, Mark
et al.

Publication Date

2023-08-29

DOI

Copyright Information

Peer reviewed

mTOR inhibition reprograms cellular proteostasis by regulating eIF3D-mediated selective mRNA translation and promotes cell phenotype switching

Sejeong Shin[1], **Min-Joon Han**[2], **Mark P. Jedrychowski**[3], **Ziyang Zhang**[4], **Kevan M. Shokat**[4], **David R. Plas**[5], **Noah Dephoure**[6], **Sang-Oh Yoon**[1,7,*]

[1]Department of Physiology and Biophysics, University of Illinois College of Medicine at Chicago, Chicago, IL 60612, USA

[2]Department of Hematology, St. Jude Children's Research Hospital, Memphis, TN 38105, USA

[3]Department of Cell Biology, Harvard Medical School, Boston, MA 02115, USA

[4]Department of Cellular and Molecular Pharmacology, University of California San Francisco, San Francisco, CA 94158, USA

[5]Department of Cancer Biology, University of Cincinnati College of Medicine, Cincinnati, OH 45267, USA

[6]Department of Biochemistry, Weill Cornell Medical College, New York, NY 10021, USA

[7]Lead contact

SUMMARY

Cells maintain and dynamically change their proteomes according to the environment and their needs. Mechanistic target of rapamycin (mTOR) is a key regulator of proteostasis, homeostasis of the proteome. Thus, dysregulation of mTOR leads to changes in proteostasis and the consequent progression of diseases, including cancer. Based on the physiological and clinical importance of mTOR signaling, we investigated mTOR feedback signaling, proteostasis, and cell fate. Here, we reveal that mTOR targeting inhibits eIF4E-mediated cap-dependent translation, but feedback signaling activates a translation initiation factor, eukaryotic translation initiation factor 3D (eIF3D), to sustain alternative non-canonical translation mechanisms. Importantly, eIF3D-mediated protein synthesis enables cell phenotype switching from proliferative to more migratory. eIF3D cooperates with mRNA-binding proteins such as heterogeneous nuclear ribonucleoprotein F (hnRNPF), heterogeneous nuclear ribonucleoprotein K (hnRNPK), and Sjogren syndrome

*Correspondence: syoon1@uic.edu.

antigen B (SSB) to support selective mRNA translation following mTOR inhibition, which upregulates and activates proteins involved in insulin receptor (INSR)/insulin-like growth factor 1 receptor (IGF1R)/insulin receptor substrate (IRS) and interleukin 6 signal transducer (IL-6ST)/ Janus kinase (JAK)/signal transducer and activator of transcription (STAT) signaling. Our study highlights the mechanisms by which cells establish the dynamic change of proteostasis and the resulting phenotype switch.

Graphical Abstract
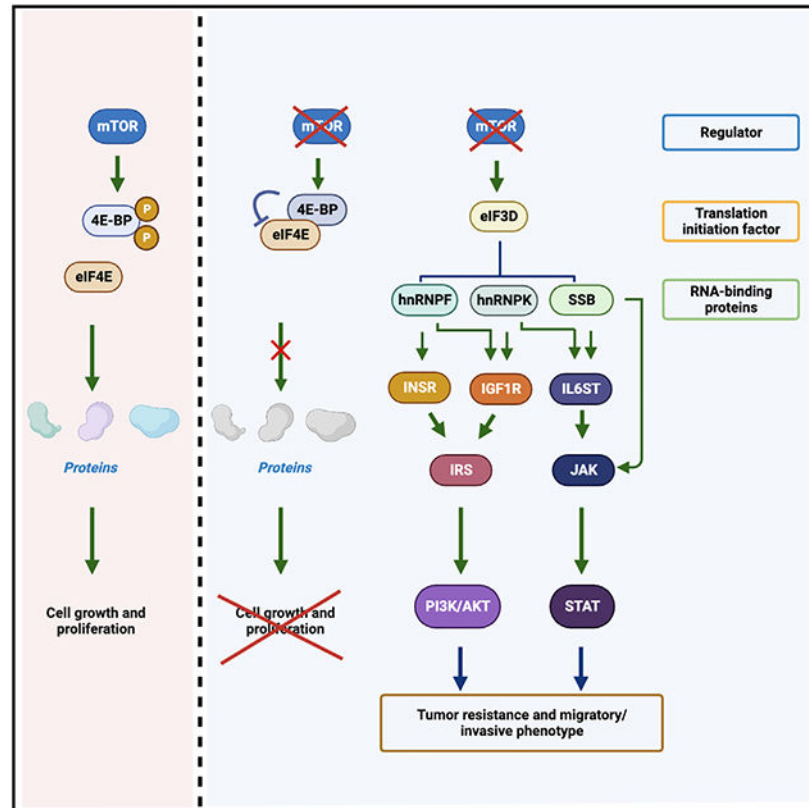
In brief

mTOR is the primary regulator of the cellular proteome, thereby governing cell growth and proliferation. Shin et al. reveal that cells dynamically change their proteome in response to mTOR inhibition by promoting eIF3D-dependent selective mRNA translation in cooperation with RNA-binding proteins while inhibiting eIF4E-mediated translation.

INTRODUCTION

Individual cells possess intricate mechanisms to create unique protein composition profiles and to dynamically alter these profiles in response to countless stimuli. The dynamic regulation of protein levels to create a state of balance is called proteostasis or protein homeostasis,[1] which is essential for the body's homeostasis. Dysregulation of proteostasis

can cause unintended levels of proteins, leading to disruption of protein homeostasis, which ultimately results in diseases such as cancer and neurological disorders.[1,2]

The mechanistic target of rapamycin (mTOR) is a central regulator of cellular proteostasis. mTOR has two complexes: mTOR complex (mTORC) 1 and mTORC2.[3] The major components of mTORC1 are mTOR and the adapter protein raptor, which provides mTOR with specificity to phosphorylate mTORC1 substrates, such as eukaryotic translation initiation factor 4E (eIF4E)-binding protein 1 (4E-BP1), S6 kinase (S6K) 1, and growth factor receptor bound protein 10 (Grb10).[3] Rapamycin-insensitive companion of mTOR (Rictor) and stress-activated protein kinase-interacting protein 1 (Sin1) are the defining components of mTORC2, which is known as the primary regulator of AKT. Both mTORCs respond to environmental cues, with mTORC1 particularly sensitive to cues such as the availability of nutrients, growth factors, hormones, and stress. mTORC1 and mTORC2 integrate these signals and accordingly regulate myriad anabolic and catabolic processes. Among these processes, mTORC1 exerts control over proteostasis through the regulation of mRNA translation and protein degradation. mRNA translation is mainly regulated at the initiation step,[4] with a significant portion of mTORC1-mediated mRNA translation initiation being mediated by the eukaryotic translation initiation factor 4F (eIF4F) complex.[5] eIF4F consists of eIF4E (a $5'$ cap-binding protein), eIF4G (a scaffolding protein), and eukaryotic translation initiation factor 4A(eIF4A; an RNA helicase). The eIF4F heterotrimer binds to the 7-methylguanosine (m^7G) $5'$ cap modification of eukaryotic mRNAs and recruits the 40S ribosomal subunit through eIF3 to initiate translation.[5] However, a family of 4E-BPs can bind eIF4E, inhibiting the eIF4F complex from initiating mRNA translation.[6,7] By directly phosphorylating and inhibiting 4E-BPs, mTORC1 plays an essential role in promoting mRNA translation (Figure 1A).[3,7,8] The ribosomal protein S6K, another substrate of mTORC1, also facilitates mRNA translation initiation by promoting the action of eIF3 and by degrading programmed cell death 4 (PDCD4), an inhibitor of eIF4A RNA helicase.[9-11] In addition to protein synthesis, mTOR also regulates protein degradation, which is mediated by two major pathways, the ubiquitin-proteasome system (UPS) and autophagy-lysosomal proteolysis. The UPS degrades individual cellular proteins that are misfolded or damaged, while autophagy is involved in the degradation of protein aggregates and whole organelles.[1,2] mTOR suppresses autophagy-mediated degradation by regulating key initiating components such as unc-51 like autophagy activating kinase 1 (ULK1) and autophagy-related protein 13 (ATG13) (Figure 1A).[12] The function of mTOR on proteasome-mediated degradation is controversial, with mTOR shown to increase[13] or decrease[14] proteasomal degradation.

Because of its role as a central regulator of cellular proteostasis, dysregulation of mTOR is directly linked to various diseases, including cancer.[15] Thus, in clinics, mTOR inhibitors such as rapamycin analogs (rapalogs) are used to treat patients with tumors and those who receive transplantation. Considering the physiological and clinical importance of mTOR and its pharmacological targeting, we were interested in determining dynamic changes in proteostasis following mTOR inhibition. We find that although mTOR inhibition blocks eIF4E-mediated translation, this inhibition also enables alternative mRNA translation largely mediated through the cooperation between the eukaryotic translation initiation factor 3D (eIF3D) and RNA-binding proteins (RBPs).

RESULTS

mRNA translation is still active when mTOR is blocked

To study mTOR feedback signaling, we used different mTOR inhibitors, rapamycin, Torin1, INK128, and RapaLink-1. Rapamycin is an allosteric inhibitor that partially blocks mTORC1. Rapamycin and its analogs efficiently inhibit mTORC1-dependent phosphorylation of S6Ks, but not 4E-BPs.[16] Torin1 and INK128, dual mTORC1/2 inhibitors, are catalytic inhibitors of mTOR that block both mTORC1 and mTORC2 completely.[17,18] Torin1 is specific to mTOR over 450 kinases tested.[19] RapaLink-1 is a bivalent inhibitor that combines the dual mTORC1/2 inhibitor INK128 (MLN0128; sapanisertib) with rapamycin through an inert chemical linker.[20] This design gives RapaLink-1 a higher avidity and makes it effective at inhibiting both wild-type (WT) mTOR and various mTOR mutants found in cancers.[20] We used different cell lines, including 621-101, an important model of human angiomyolipoma, a condition that is responsive to mTOR inhibitors in the clinic.[21]

Using these mTOR inhibitors, we investigated the levels of cyclin D3, a protein whose expression is regulated by eIF4E-mediated cap-dependent translation.[22] Dual mTORC1/2 inhibition by Torin1 or RapaLink-1 decreased cyclin D3 levels in 4E-BP1/2 WT cells, but not in 4E-BP1/2 knockout (KO) cells (Figure 1B), consistent with mTOR inhibition blocking eIF4E-mediated translation through 4E-BP1/2.[22] As expected, rapamycin, a partial mTORC1 inhibitor, did not suppress 4E-BP1 phosphorylation or cyclin D3 expression (Figures 1B and S1A). mRNA translation is essential for cell proliferation. As shown in Figures 1C and S1B, mTOR inhibitors, especially dual mTORC1/2 inhibitors, and cycloheximide, an mRNA translation inhibitor, dramatically decreased cell proliferation. However, cell numbers still increase in the presence of dual mTORC1/2 inhibitors, suggesting that inhibition of mTOR-mediated mRNA translation is ineffective at blocking cell proliferation completely. We, therefore, wondered how effective mTOR inhibition is for blocking mRNA translation. For this, we measured nascent protein synthesis after mTOR inhibition. As shown in Figure 1D, cycloheximide completely blocked mRNA translation. Although dual mTORC1/2 inhibition dramatically reduced protein synthesis, mRNA translation machinery was still active (Figure 1D). Rapamycin did not show a profound effect on new protein synthesis (Figure 1D). Taken together, these data suggest that cells can still induce an mRNA translation mechanism in response to the inhibition of mTOR, a major regulator of mRNA translation. We, therefore, examined the effect of mTOR inhibition on proteome composition using a quantitative proteomics approach. Among about 7,650 proteins quantified, we analyzed around 6,650 proteins, excluding those quantified by only one peptide, to minimize errors in data analysis. Among these, we identified 101 (1.5%), 729 (11%), and 727 (11%) differentially expressed proteins ($\mathrm{Log}_{-1.5}$(fold change) > 1 or < −1, adjusted p < 0.05) by treatment with rapamycin, Torin1, and RapaLink-1, respectively (Figure 1E). We first analyzed proteins downregulated by dual mTORC1/2 inhibitors, Torin1 and RapaLink-1. Around 83% and 84% of proteins downregulated by Torin1 and RapaLink-1, respectively, overlap (Figure S1C), and some examples are shown in Figure 1F. These indicate that these two inhibitors function similarly as dual mTORC1/2 inhibitors, although their structures are quite different. Despite a more modest effect on

the proteome by rapamycin (Figures 1E), 81% of proteins downregulated by rapamycin overlapped with those also downregulated by Torin1 or RapaLink-1 (Figure 1G). Because rapamycin did not induce dephosphorylation of 4E-BP1, the observed downregulation of proteins following rapamycin treatment is likely not through inhibition of eIF4E-dependent mRNA translation. Interestingly, mTOR inhibition also upregulated proteins. Around 77% and 76% of proteins upregulated by Torin1 and RapaLink-1, respectively, overlap (Figure S1D), and some examples are shown in Figure 1H. Around 90% of upregulated proteins by rapamycin also were upregulated by Torin1 and/or RapaLink-1 (Figure 1I). Taken together, these data suggest that although mTOR is a major positive regulator of mRNA translation, and thus mTOR inhibition blocks protein synthesis, cells still synthesize proteins in response to mTOR inhibition.

Proteome changes downstream of mTOR inhibition are largely independent of changes in corresponding mRNA levels

We were next interested in any transcriptome changes following mTOR inhibition that might contribute to the observed upregulation or downregulation of proteins. Using next-generation RNA sequencing, we obtained information on global changes of around 15,000 RNAs, including mRNAs and non-coding RNAs. Among these, we identified 397 (3%), 2,548 (17%), and 2,215 (15%) differentially expressed RNAs (Log_2(fold change) > 1 or < -1, adjusted $p < 0.05$) by treatment with rapamycin, Torin1, and RapaLink-1, respectively (Figure 2A). We first analyzed downregulated transcripts. As shown in Figure 2B, around 74% and 83% of mRNAs downregulated by Torin1 and RapaLink-1, respectively, overlap each other. Some examples are shown in Figure 2C. Also, 80% of mRNAs downregulated by rapamycin are also downregulated by Torin1 or RapaLink-1 (Figure 2D). There were also a number of mRNAs that were upregulated following treatment with mTOR inhibitors. Around 69% and 85% of mRNAs upregulated by Torin1 and RapaLink-1, respectively, overlap each other (Figure 2E). Some examples are shown in Figure 2F. Also, 88% of mRNAs upregulated by rapamycin are also upregulated by Torin1 or RapaLink-1 (Figure 2G). Because the three mTOR inhibitors used have highly divergent structures, the high level of overlap in these datasets suggests that these three mTOR inhibitors affect mTOR activity quite selectively. We then analyzed around 6,300 mRNAs, which encode proteins that were seen in proteome analysis. As shown in Figures 2H and 2I, more than 80% of proteins that were downregulated (Figure 2H) or upregulated (Figure 2I) following rapamycin treatment did not show dramatic changes in mRNA levels. In the case of dual mTORC1/2 inhibition, around 30% of proteins that showed perturbed levels had corresponding mRNA changes (Figures 2H and 2I), suggesting that about 70% of the protein expression changes following Torin1 or RapaLink-1 treatment could not be attributed to changes in mRNA levels. Along with the data on proteins whose levels were not changed following mTOR inhibition (Figure S2), these all indicate that transcriptome alterations do not solely explain changes of the cellular proteome caused by mTOR inhibition. In addition, how an increase in mRNA would lead to an increase in protein expression under mTORC1/2 blockade is hard to explain, given that mTOR inhibition leads to suppression of eIF4F-mediated cap-dependent mRNA translation.

mTOR inhibition increases protein levels of INSR, IGF1R, and IRS and activates INSR/IGF1R/IRS regulatory complex and its downstream AKT signaling

Analysis of downregulated proteins from both Torin1 and RapaLink-1 conditions revealed these proteins belong to pathways involved in DNA metabolism, cell-cycle progression, and cholesterol biosynthesis (Figure 3A). Although the downregulated proteins are interesting themselves, we were more interested in proteins upregulated by mTOR inhibition based on our hypothesis that protein upregulation may be responsible for cell survival following mTOR inhibition. Analysis of upregulated proteins by both Torin1 and RapaLink-1 revealed proteins involved in peptidase/proteolysis and enzyme-linked receptor protein signaling pathway (Figure 3B). Further examination using interaction enrichment analysis revealed many of these upregulated proteins belong to directly interacting protein networks, including the proteins involved in the insulin receptor (INSR)/insulin-like growth factor 1 receptor (IGF1R) pathway, such as INSR, IGF1R, and IRS1/IRS2 (Figure 3C). We confirmed that dual mTORC1/2 inhibition (Figures 3D and S3A) and mTOR knockdown (Figures 3E and S3B) led to an increase in their levels and fibroblast growth factor receptor (FGFR) (Figure S3C).

We were then curious whether mTOR inhibition would impact the phosphorylation status and, therefore, the activity of INSR/IGF1R. As shown in Figures 3F, 3G, S3D, and S3E, dual mTORC1/2 inhibition and mTOR knockdown increased total and phosphotyrosine levels of IGF1R and INSR, in which phospho-IGF1R antibody also binds to phosphorylated INSR. In the case of IRS, while tyrosine phosphorylation at Y608 (mouse)/Y612(human) increases its activity,[23] serine phosphorylation at S636/S639 is known to inhibit its activity.[24] As shown in Figures 3H, S3F, and S3G, the serine phosphorylation of IRS1 decreased, but tyrosine phosphorylation was increased after dual mTORC1/2 inhibition. All these data suggest that dual mTORC1/2 inhibition upregulates and activates INSR/IGF1R/IRS.

We and others showed that long-term inhibition of mTORC1/2 by Torin1 led to hyperactivation of AKT activity in mTOR targeting drug-resistant cell lines by increasing phosphorylation at Thr308 (activation loop) by 3-phosphoinositide-dependent kinase 1 (PDK1),[25,26] as well as by inducing mTORC2-independent phosphorylation at S473 (hydrophobic motif),[26] although mTORC1/2 dual inhibition completely blocked both mTORC1 and mTORC2. As shown in Figure S3H, 4-h treatment with dual mTORC1/2 inhibitors blocked AKT phosphorylation profoundly. However, expectedly, 24-h treatment with dual mTORC1/2 inhibitors, Torin1 and RapaLink-1, did not inhibit AKT phosphorylation dramatically even though these inhibitors completely blocked the phosphorylation of mTORC1 substrates S6K1 and 4E-BP1 (Figures 3I and S3I-S3L). In agreement with these findings, mTOR knockdown also led to increased AKT phosphorylation (Figures 3J, S3M, and S3N). We next used Rictor KO cells to specifically block mTORC2 activity. As shown in Figures 3K, S3O, and S3P, Rictor KO cells in growing conditions display a decrease in S473 phosphorylation compared with WT, suggesting that mTORC2 is crucial for AKT phosphorylation under growing conditions. However, the fact that dual mTORC1/2 inhibition did not abolish AKT phosphorylation in WT cells and the finding of increased phospho-AKT levels by dual mTORC1/2 inhibition in Rictor KO cells compared with control confirms that AKT phosphorylation at S473 following dual

mTORC1/2 inhibition is not dependent on mTORC2. These findings and our previous report[26] suggest that dual mTORC1/2 inhibitors, although effective at blocking mTOR activity, cause feedback signaling, which allows for mTORC2-independent activation of AKT.

As shown in Figure S3Q, all dual mTORC1/2 inhibitors in our study increased the levels and activities of INSR/IGF1R and upregulated Akt phosphorylation. We obtained the same results with mTOR inhibition for 48 h when mTORC1 activity is still blocked (Figure S3R). The receptor tyrosine kinase (RTK)/phosphatidylinositol 3-kinase (PI3K) pathway is major signaling that activates AKT. We found that RTKs such as INSR, IGF1R, and FGFR are upregulated by mTOR inhibition. We tested the role of RTKs in the mTOR-inhibition-induced increase in AKT phosphorylation. We used various RTK inhibitors in combination with dual mTORC1/2 inhibition and found that INSR/IGF1R inhibition blocked the mTOR-inhibition-induced increase in AKT phosphorylation at both the activation loop and hydrophobic motif (Figures 3L, 3M, S3S, and S3T). Similarly, INSR/IGF1R inhibitors blocked mTOR-inhibition-mediated glycogen synthase kinase 3β (GSK3β) phosphorylation at the AKT site (Figure 3N), which suggests that AKT activation is mainly mediated by INSR/IGF1R signaling. Taken together, these suggest that mTOR inhibition induces upregulation and activation of INSR/IGF1R/IRS signaling, which mediates Akt activation.

mTOR inhibition activates the JAK/STAT pathway by increasing the levels of proteins involved in this signaling

In addition to IRS/PI3K/AKT signaling, we were also interested in JAK/STAT signaling because these two pathways are the main signalings initiating from INSR/IGF1R and are critical for cell growth, proliferation, and migration.[27] We found that JAK2 protein levels and tyrosine phosphorylation at Tyr1007/1008 (Figures 4A, 4B, S4A, and S4B), an indicator of JAK2 activity, were increased by dual mTORC1/2 inhibition or mTOR knockdown. We performed a mini-phosphorylation analysis and found that phosphorylation of STAT3 at Tyr705, a key site for STAT3 activation, which is known to be modified by JAK2, was increased by dual mTORC1/2 inhibitors, but not by rapamycin (Figure S4C). We examined this phosphorylation using immunoblot analysis and confirmed its increase by mTOR inhibitors or knockdown (Figures 4C, 4D, S4D, and S4E). Using JAK inhibitors, we also found that mTOR-inhibition-mediated JAK activation was involved in STAT3 phosphorylation (Figures 4E and S4F). We then wondered whether the increase in JAK2 phosphorylation by mTOR inhibition was mediated by INSR and IGF1R. Unlike our expectation, INSR/IGF1R inhibition did not block JAK2 phosphorylation induced by mTOR inhibition (Figures 4F and S4G). JAK signaling is known to be initiated downstream of growth factor receptor and cytokine receptor activation. However, JAK2 phosphorylation was not reduced by inhibition of other growth factor receptors (Figure 4G), suggesting that cytokine receptors, not RTKs, may mediate JAK signaling following mTOR inhibition. We selected several candidates using the data analysis from proteome, phospho-proteome, and transcriptome. After testing them, we identified IL-6ST (glycoprotein 130: gp130) as an important mediator of JAK2 activation following mTOR inhibition. IL-6ST is a transmembrane receptor that serves as a signal transducer of various cytokines, including

IL-6, IL-11, and oncostatin M, in which IL-6ST binds to and activates JAK.[28] We found that mTOR inhibition increased the IL-6ST protein levels (Figure 4H), and inhibition of IL-6ST blocked the phosphorylation of JAK2 induced by mTOR inhibition (Figure 4I). STAT3 is a transcription factor, and the IL-6 promoter has a STAT binding site. Also, there is a positive feedback loop between IL-6, JAK, and STAT.[29] As shown in Figure 4J, IL-6 mRNAs were upregulated by mTOR inhibition but downregulated by STAT3 inhibition. These findings suggest that mTOR inhibition activates IL-6ST/JAK/STAT/IL-6 signaling.

Inhibition of mTOR leads to the activation of eIF3D-dependent mRNA translation

Considering mTOR has been regarded as a positive regulator of anabolism and a negative regulator of catabolism, it is surprising that mTOR inhibition by dual mTORC1/2 targeting drugs and knockdown led to the upregulation of select proteins. One possible mechanism to explain this would be through the release from proteasomal degradation. It is known that mTORC1 promotes proteasome-dependent degradation of IRS by increasing its Ser/Thr phosphorylation.[30,31] In line with this model, complete mTOR inhibition with dual mTORC1/2 inhibitors increased IRS levels (Figures 3D, 3E, and 3H). In contrast with IRS, we found that mTOR increased Grb10 stability, with rapamycin inducing Grb10 proteasomal degradation[32] and mTOR inhibitors and knockdown decreasing Grb10 protein levels (Figure 5A). Therefore, mTOR inhibition can either impede or promote proteasomal degradation of targets to upregulate or downregulate expression, respectively. However, little is known about how the levels of other proteins in our study involved in INSR/IGF1R and IL-6ST (gp130)/JAK signaling are regulated by mTOR. To study this, we first examined mRNA levels of RTKs whose protein levels were increased by mTOR inhibition. Given that significant mRNA upregulation is set as $\mathrm{Log_2}$(fold change) > 1, their mRNA levels were not substantially increased following mTOR inhibition (Figure 5B). Specifically, IGF1R mRNA levels did not reach the threshold for significant increases at any time point during treatment (Figure 5C), although IGF1R protein levels were still upregulated following 24-h (Figures 3D, 3F, and S3Q) and 48-h (Figure S3R) treatment with mTOR inhibitors. As in the global analysis of mRNA levels and protein levels (Figures 2H and 2I), these results suggest that mRNA levels cannot fully explain protein levels. We next used the general mRNA translation inhibitor cycloheximide and found that INSR and IGF1R levels were not increased by mTOR inhibition in the presence of cycloheximide, suggesting that their upregulation may be through mRNA translation (Figures 5D and S5A).

Our main question was how mTOR inhibition could increase mRNA translation when the eIF4F-dependent translation was blocked. Dual mTORC1/2 inhibition completely blocked 4E-BP1 phosphorylation, indicating inhibition of eIF4E, the primary regulator of cap-dependent translation. Because we observed nascent protein synthesis in the presence of mTOR inhibitors (Figure 1D), we hypothesized that inhibition of this eIF4F-dependent translation could lead to compensatory activation of eIF4F-independent modes of mRNA translation. We first tested whether 4E-BP-dependent eIF4E inhibition is required to induce upregulation of proteins when mTOR activity is blocked. For this, we performed quantitative proteomics using 4E-BP1/2 WT and 4E-BP1/2 null mouse embryonic fibroblasts (MEFs). As in the examples shown in Figure 5E, dual mTORC1/2 inhibition led to the downregulation of proteins in WT cells, including collagens and cyclin

D3 (CCND3), but the same treatment in 4E-BP1/2 null cells produced a much smaller change, in line with mTOR regulating translation primarily through 4E-BP/eIF4F-mediated translation. Some proteins were downregulated by dual mTORC1/2 inhibition in both WT and 4E-BP1/2 null cells, suggesting that additional mechanisms, independent of 4E-BP/eIF4E, are involved in this regulation (Figure 5F). Some of this regulation may be taking place post-translationally as in the case of Grb10 (Figures 5A and 5G), whereby we showed that mTOR inhibition promotes Grb10 proteasomal degradation.[32] We next investigated the upregulation of proteins following mTOR inhibition and found proteins involved in INSR/IGF1R/IRS and IL-6ST (gp130)/JAK2 signaling to be upregulated in both WT and 4E-BP1/2 null cells (Figures 5G and 5H). This suggests that the upregulation of these proteins is not induced by the inhibition of eIF4E-mediated cap-dependent translation. eIF4E interaction with eIF4G, a scaffold protein that recruits eIF4A helicase and eIF3/43S pre-initiation complex,[5] is required to initiate cap-dependent translation. We used eIF4E/eIF4G inhibitor 1 (4EGI-1) to inhibit the interaction between eIF4G and eIF4E (Figure 5I), which suppresses eIF4E-mediated cap-dependent translation. Treatment with 4EGI-1 did not block mTOR-inhibition-mediated upregulation of IGF1R (Figure 5I). We also knocked down the major forms of eIF4E and eIF4G, eIF4E1 and eIF4G1, and found that their decrease did not significantly inhibit the upregulation of IGF1R or INSR following mTOR inhibition (Figures S5B and S5C). Isoforms of eIF4E and eIF4G, such as eIF4E2 and eIF4G2 (DAP5), are known to regulate the translation of general or specific mRNA species.[33-35] However, the knockdown of eIF4E2 (Figure S5D) and eIF4G2 (DAP5) (Figure S5E) did not block mTOR-inhibition-induced IGF1R expression.

We next directed our attention to the multi-subunit eIF3 complex. eIF3 is well-known for its role in general mRNA translation[36]; however, evidence is accumulating that eIF3 subunits are also engaged in non-canonical and selective mRNA translation aseIF4 molecules.[36] Thus, we investigated whether any eIF3 subunits are responsible for the upregulation of proteins following mTOR inhibition. Interestingly, of several components we tested, we found that knockdown of eIF3D (Figures 5J and S5F), but not eIF3B (Figure S5G), eIF3K (Figure S5H), and eIF3I (Figure S5I), significantly blocked mTORC1/2-inhibition-induced upregulation of INSR, IGF1R, IL-6ST, and JAK2. eIF3D knockdown did not block the upregulation of IRS and PDCD4 following mTOR inhibition (Figure 5K), which agrees with that their levels are regulated by mTOR-mediated protein degradation.[11,31] We also found that tyrosine phosphorylation of IGF1R, an indicator of IGF1R activity, was decreased in eIF3D knockdown cells following mTOR inhibition (Figures 5L and S5J).

eIF3D cooperates with RBPs to promote selective mRNA translation when mTOR activity is inhibited

Our results suggest that eIF3D mediates selective mRNA translation when mTOR is inhibited. To gain more direct evidence, we performed RNA immunoprecipitation (RIP) to test whether eIF3D binds to the mRNA species we found to have increased translation under mTOR inhibition. Analysis of the RIP data showed that INSR, IGF1R, FGFR1, IL-6ST, and JAK2 mRNAs bind to eIF3D protein significantly compared with control, and that this interaction, except IL-6ST mRNA, is increased when mTOR is inhibitec (Figures 6A and S6A). We next performed eIF3D interactomics to identify molecules cooperating with

eIF3D to promote mRNA translation under mTOR-inhibited conditions and found several proteins that interacted with eIF3D in an mTOR-inhibitor-dependent manner. Interestingly, some identified proteins (Figure 6B), heterogeneous ribonuclear protein F (hnRNPF), heterogeneous nuclear ribonucleoprotein K (hnRNPK), and SSB (La autoantigen), are mRNA *trans*-acting factors that bind to mRNAs and regulate mRNA translation.[37] We first analyzed interacting molecules ol these RBPs when mTOR is inhibited. The functional enrichment analysis reveals that the major function of their interacting proteins, which include other RBPs, ribosomes, and TIFs (Figures S6B-S6D), is RNA metabolism (Figures 6C-6E). We then investigated whether hnRNPF, hnRNPK, and SSB regulate the levels of the proteins in this study. Intriguingly, each of these proteins had a unique but somewhat overlapping effect on the expression of proteins. As shown in Figures 6F-6K, hnRNPF knockdown affected levels of IGF1R, INSR, and FGFR, but not IL-6ST and JAK2. hnRNPK knockdown reduced expression ol IGF1R, FGFR, IL-6ST, and JAK2 induced by mTOR inhibition. SSB knockdown significantly blocked the upregulation of IL-6ST and JAK2 when mTOR is inhibited but did not affect IGF1R, INSR, and FGFR expression. To investigate whether binding of eIF3D to mRNAs was affected by these RBPs, we performed RIP using RBP knockdown cells. Analysis of the RIP data showed that the binding of INSR, IGF1R, FGFR1, IL-6ST, and JAK2 mRNAs to eIF3D was profoundly decreased by the knockdown of RBPs (Figure 6L). Using the RBP knockdown cells, we also measured the levels of mRNAs in this study. Although the RBP knockdown decreased mRNA levels, the effects were not as dramatic as those observed in RIP (Figure 6M). Together, these findings suggest that when mTOR is inhibited, eIF3D, a TIF, cooperates with its interacting partners, especially RBPs, to upregulate proteins involved in INSR/IGF1R and IL-6ST/JAK signaling, and these RBPs are involved in the further selection of mRNAs.

mTOR inhibition mediates eIF3D-dependent phenotypic switching from proliferative to migratory

Interested in this finding, we performed quantitative proteomics using control and two different eIF3D short hairpin RNAs (shRNAs) to identify additional proteins regulated by eIF3D during mTOR inhibition. In addition to the molecules we identified, such as IGF1R and IL-6ST, eIF3D knockdown blunted or blocked increases in approximately half of the proteins that were upregulated by mTOR inhibition, and examples are shown in Figure 7A. We also found that FGFR, which was identified in interaction enrichment analysis (Figure 3C), was upregulated in an eIF3D-dependent manner (Figure S7). The other half of the proteins were upregulated in an eIF3D-independent manner following mTOR inhibition. As shown in examples in Figure 7B, this group also includes IRS, which we found to be regulated by mTOR-mediated degradation, suggesting that upregulated proteins in this group following mTOR inhibition are at least partly regulated by suppression of degradation. Analysis of eIF3D-dependent upregulation of proteins showed that many upregulated proteins are involved in cell migration and related processes, such as cell-matrix adhesion, cell morphogenesis, and actin dynamics (Figure 7C). Analysis of the proteins showing eIF3D-independent upregulation revealed enrichment of proteins involved in carbohydrate-derivative catabolism, lipid breakdown, lysosome organization, and autophagy (Figure 7D), suggesting that degradation of molecules such as lipids and proteins is one of the functions of eIF3D-independent upregulation of proteins following mTOR inhibition.

mTOR is known as a major regulator of cell growth and proliferation. Correspondingly, mTOR inhibition reduces cell proliferation dramatically. However, surprisingly, our results show that mTOR inhibition upregulates proteins involved in cell migration, suggesting that once cancer cells become resistant to dual mTORC1/2 inhibition, they promote cell motility. As shown in Figures 7E and 7F, A375 cells, invasive cancer cells, that were preincubated with dual mTORC1/2 inhibitors for 48 h showed a marked increase in migration and invasion in the presence of mTORC1/2 inhibitors during the assay. INSR/IGF1R/AKT signaling and JAK/STAT signaling are well-known for increasing cell migratory and invasive potential.[27,38] We used inhibitors of those signaling networks and found them able to inhibit cell migration (Figures 7G and 7H) and invasion (Figures 7I and 7J) induced by mTOR inhibition. These findings suggest that although mTOR inhibition reduces cell proliferation partly through 4E-BP1/eIF4E-dependent mRNA translation, mTOR inhibition simultaneously induces cell motility through eIF3D-dependent mRNA translation.

DISCUSSION

mRNA translation is a complex process that requires orchestrated coordination between mRNAs, ribosomes, aminoacyl-tRNAs, and *trans*-acting molecules such as translation initiation, elongation, and termination factors and other RBPs.[5] mRNA translation is mainly regulated at the initiation step.[5,9,39] Therefore, TIFs, including eIF3 and eIF4, are essential regulators of mRNA translation efficiency. This study specifically investigated the link between eIF4F, eIF3, and mTOR. It has been thought that most mRNA TIFs are involved in general global mRNA translation. However, growing evidence indicates that initiation factors regulate the translation of specific transcripts leading to selective mRNA translation depending on the cellular context. For example, isoform-specific functions of eIF4F factors, such as eIF4G2 (DAP5), in the translation of specific sets of mRNAs are becoming recognized more recently and are of great interest from both basic science and therapeutic standpoints.[33-35,40-42] The existence of alternative eIF4F components provides a reasonable explanation as to how cells maintain protein production capacity in the absence or inhibition of the canonical eIF4F.[35] Like the eIF4F complex, the eIF3 complex, which recruits the 43S preinitiation complex containing a small ribosomal subunit to the 5′ cap bound eIF4F,[5] has also been regarded as a general global TIF complex for cap-dependent translation.[36] However, growing evidence suggests that in addition to its role in global translation, eIF3 can be customized with variant components to contribute to the translation of specific mRNA transcripts.[34,36]

The eIF3 complex is composed of 12 subunits: eIF3A-I, K, L, and M.[36,43] Of note, albeit eIF3J was initially considered to be an integral part of the eIF3 complex, mounting evidence shows that it mostly acts independently of eIF3.[34,36,44] Specific mRNAs rely on different subunits of eIF3 for their translation; therefore, specific subunits allow for the specialization of the eIF3 complex to promote the translation of select sets of mRNAs instead of global cap-dependent initiation.[34,43,45] However, not much is known about the subunit-specific functions of eIF3, including the exact stimuli that induce them and what transcripts they regulate. Among eIF3 subunits, eIF3D functions as an intermolecular bridge between eIF3 and 40S ribosomal subunit.[46] Although eIF3D knockdown affects cell proliferation, this knockdown does not regulate protein levels of other eIF3 subunits or the integrity of

the eIF3 complex.[47] Thus, it has been suggested that instead of being involved in the general translation of eIF3, eIF3D may promote the translation of specific mRNAs whose proteins play vital roles in cells.[43,47-49] A recent report shows that transforming growth factor β (TGF-β) induces T cell differentiation through regulation of eIF4G2 (DAP5)/ eIF3D-dependent mRNA translation when mTORC1 is partially inhibited by rapamycin, but not when it is fully inhibited by dual mTORC1/2 inhibitor.[50] Also, eIF3D induces cap-dependent translation of Jun and the mTORC1 subunit raptor under glucose-deprived, but not serum- or glutamine-deprived, conditions.[51] Furthermore, eIF3D appears to play a major role in the reactivation of translation during the chronic phase of integrated stress response caused by endoplasmic reticulum (ER) stress.[49] Our results suggest that the eIF3D provides an alternative translation system for specific sets of mRNAs during proteostasis stress induced by mTOR inhibition.

Changes in mRNA levels do not always correlate with corresponding protein levels. For instance, although stress conditions such as hypoxia, nutrient deprivation, and anti-cancer drug treatment, including mTOR inhibitor treatment in our study, can increase the transcription of stress-induced genes, protein levels may not always increase.[52-54] This phenomenon arises from a buffering mechanism in translation that maintains constant protein levels despite fluctuations in mRNA levels.[55] In addition, certain proteins are upregulated or downregulated without significant changes in their corresponding mRNAs. The discrepancy between mRNA and protein levels can be attributed to several factors, including translational efficiency and protein degradation rates in cells.[52,53] Translational efficiency is determined by a complex process that requires orchestrated coordination of resources such as energy, nutrients (e.g., amino acids), *cis*-acting factors (mRNAs), and *trans*-acting factors that include ribosomes, tRNAs, translation initiation/elongation/ termination factors, and other RBPs.[52,53] This suggests that mRNA translation efficiency and protein levels cannot be solely determined by the levels of *cis*-acting factors (mRNAs). Instead, the availability and modification of these resources, which rely on intra- and extra-cellular environments, are critical for the regulation of protein levels. Thus, lack of energy, RNA modification, and/or inhibition of the mRNA translation system under stress conditions, for example, explain the discrepancy between mRNA levels and protein levels.[52-54] Among these resources governing mRNA translation, we were interested in *trans*-acting factors such as TIFs and other RBPs. Each RBP usually has multiple RNA-binding domains, which have specific binding modalities with mRNAs, and therefore tend to bind to mRNAs selectively. It is also known that each different mRNA has distinct RBPs and even the same mRNAs with different cellular contexts giving rise to varying combinations of RBP binding, allowing for complex but specific regulation of the mRNAs.[56] We have found that the TIF eIF3D interacts with RBPs such as hnRNPF, hnRNPK, and SSB (La autoantigen) in which these RBPs provide further specificity to mRNA translation in addition to that afforded by eIF3D. Our data indicate that cooperation between the *trans*-acting factors, especially between TIFs and RBPs, is essential for efficient and transcript-specific mRNA translation to adapt or escape stress conditions.

In cancer, the INSR/IGF1R and JAK/STAT signaling pathways induce cancer survival and phenotype switching through increased stemness characterized by decreased proliferation and increased cell motility and resistance to stress.[27,57] Our current and previous findings

show that mTOR inhibition synergistically activates INSR/IGF1R/IRS/AKT signaling networks by inducing (1) cooperation of eIF3D and RBPs for INSR/IGF1R protein synthesis and inhibition of IRS degradation (Figures 5 and 6); (2) integrin adhesome/focal adhesion complex-mediated activation of INSR/IGF1R;[26] and (3) degradation of a cellular INSR and IGF1R inhibitor, Grb10.[32] We also show that mTOR inhibition induces eIF3D- and RBP-mediated IL-6ST (gp130)/JAK/STAT signaling, which is involved in autoimmune disease, malignancy, and cancer stemness.[57] Overall, our findings suggest that following mTOR inhibition, cells undergo dynamic and fine-tuned proteostasis changes that regulate specific signaling networks by (1) inhibiting eIF4E/4E-BP1-dependent mRNA translation to suppress cell proliferation and (2) stimulating eIF3D-mediated INSR/IGF1R/IRS/PI3K and gp130/JAK/STAT signaling for cooperative effects on cell motility and stress resistance. These findings are consistent with previous observations that, akin to hypoxia, mTOR inhibitors cause translational reprogramming that selectively induces the levels of NANOG, SNAIL, and NODAL proteins and increases the plasticity of breast cancer cells.[58]

It has long been known that mTOR is positively involved in anabolism by promoting protein synthesis and negatively involved in catabolism by inhibiting autophagy-mediated protein degradation. Our study shows that when mTOR is inhibited, cells shut down eIF4F-dependent mRNA translation but operate selective mRNA translation in addition to selective protein stabilization or degradation mechanisms to dynamically change their proteome, which induces phenotype switching and stress resistance. This suggests that mTOR is a key molecule for cellular proteostasis and phenotype determination by regulating anabolism and catabolism simultaneously to dictate cell fate. Selective and targeted protein stabilization/degradation has the potential to be a critical therapeutic target node to treat diseases, including neurological disorders, aging, and cancer that are characterized by an excess of disease-promoting proteins. A combined strategy using inhibitors against selective protein synthesis and selective stabilization/degradation holds promise as a tool for combating diseases. Progressing far from its original clinical use as an organ transplant anti-rejection drug, the use of mTOR inhibitors is currently a promising and validated strategy in clinics to target many types of cancer and other diseases such as *tuberous sclerosis complex* (TSC) that shows a high risk of causing epilepsy and autism. Considering the physiological function of mTOR as a key regulator of cell metabolism, cell proliferation, and survival and the clinical importance of mTOR targeting, our studies provide invaluable insight into mTOR's feedback signaling, proteome remodeling, and phenotype switching that can be translated into clinical application.

Limitations of the study

mRNA translation is controlled by a combination of cellular resources, including energy, nutrients, mRNAs, ribosomes, tRNAs, TIFs, and other RBPs. Thus, depending on the expression profile of mRNAs, TIFs, and RBPs in a given cell type, in addition to the availability of energy and nutrients under certain conditions, different cells and different inner and outer cellular environments may exert distinct changes in mRNA translation efficiency. This can result in unique adaptive proteome profiles between different tissue and cell types to the same stress, such as mTOR inhibition.

STAR★METHODS

RESOURCE AVAILABILITY

Lead contact—Further information and requests for resources and reagents should be directed to and will be fulfilled by the lead contact, Sang-Oh Yoon (syoon1@uic.edu).

Materials availability—Newly generated materials associated with this manuscript are available from the lead contact without restrictions.

Data and code availability

- Proteomics and RNA-seq data have been deposited to PRIDE and GEO with accession numbers PXD041933 and GSE229623, respectively.

- This paper does not report original code.

- Any additional information required to reanalyze the data reported in this paper is available from the lead contact upon request.

EXPERIMENTAL MODELS AND STUDY PARTICIPANT DETAILS

Cell lines—Melanoma cell line, A375, was obtained from ATCC. 621-101 cells were kindly provided by Dr. Jane Yu (University of Cincinnati, OH). 4E-BP1&2 WT and KO MEFs were generously provided by Dr. Nahum Sonenberg (McGill University, Canada). Rictor WT and KO MEFs were kindly provided by Dr. Brendan Manning (Harvard Medical School, MA). 293T cells and lentiviral packaging and envelope plasmids were generous gifts from Dr. Andrew L. Kung (Memorial Sloan Kettering Cancer Center, NY) and Dr. David Baltimore (California Institute of Technology, CA). MEFs and melanoma were maintained in DMEM containing 10% FBS at 37°C with 5% CO_2. 621-101 cells were grown in DMEM/F12 media supplemented with 10% FBS, 50 nM sodium selenite, 25 μg/mL insulin, 200 nM hydrocortisone, 10 μg/mL transferrin, 1 nM triiodothyronine, 10 μU/ml vasopressin, 10 nM cholesterol, 1.6 μM ferrous sulfate, and 20 ng/mL EGF.

METHOD DETAILS

Reagents—Anti-phospho-S473-AKT, anti-phospho-T308-AKT, anti-AKT, anti-phospho-4E-BP1, anti-4E-BP1, anti-4E-BP2, anti-phospho-S6K1, anti-S6K1, anti-phospho-S6, anti-S6, anti-phospho-IGF1R, anti-IGF1R, anti-INSR, anti-phospho-Ser636/639-IRS1, anti-IRS1, anti-IRS2, anti-phospho-JAK2, anti-JAK2, anti-phospho-Stat3, anti-mTOR, anti-Rictor, anti-PDCD4, anti-eIF4E, anti-eIF4E2, anti-eIF4G, anti-eIF4G2, anti-cyclin D3, anti-FGFR, anti-SSB (La), anti-phospho-GSK3β, anti-GSK3β, anti-GP130 (IL6ST), and anti-Grb10 antibodies were purchased from Cell Signaling Technology. Anti-Stat3, anti-hnRNPK, and anti-hnRNPF antibodies were obtained from Proteintech. Anti-eIF3D was from Santa Cruz, and anti-eIF3B and anti-Grb10 antibodies were from Novus Biologicals. An anti-eIF3K antibody was purchased from Abclonal. Anti-actin and anti-phospho-Tyr612-IRS1 antibodies, cycloheximide, SC144, qPCR primers, lentiviral shRNAs, and imprint RNA immunoprecipitation (RIP) were obtained from Sigma. Biocoat Matrigel invasion chamber, cell culture inserts, and collagen I were purchased from Corning, Falcon, and Gibco, respectively. Rapamycin, Torin1, sapanisertib, erlotinib, BMS754807,

infigratinib, crenolanib, ruxolitinib, momelotinib, 4EGI-1, and C188-9 were purchased from Selleckchem. Click-iT AHA (l-Azidohomoalaine), tetramethylrhodamine (TAMRA) Alkyne, and Click-iT protein reaction buffer kit were obtained from Invitrogen and Click Chemistry Tools. The protease inhibitor cocktail and phosphatase inhibitor cocktail are from Thermo Scientific.

Plasmids and generation of stable cells—Lentivirus was generated as described previously.[26] Shortly, shRNA plasmids or overexpression plasmids were transfected into 293T cells using Lipofectamine 2000 (Thermo Fisher Scientific) with the expression plasmids for packaging (8.9) and envelope (VSVG), and the medium was changed the next day. After ~30 h, viral supernatants were harvested, and the new medium was added. Viral supernatants were collected the next day. Cells were infected with viral supernatants in the presence of a serum-containing medium supplemented with 8 μg/mL polybrene. The viral-containing medium was removed after 24 h, and cells were grown in serum-containing media for another day. Cells were then treated with puromycin (A375: 2 μg/mL, MEFs: 4 μg/mL, 621-101: 10 μg/mL) for selection. The knockdown efficiency was confirmed by immunoblot analysis.

Immunoblot analysis—Immunoblot analysis was performed as described previously.[59] Cells were extracted in lysis buffer containing Triton X-100 (25 mM HEPES (pH 7.4), 150 mM NaCl, 1% Triton X-100, 5 mM EDTA, 1 mM EGTA, 10 mM β-glycerophosphate, proteases inhibitor cocktail, and phosphatase inhibitor cocktail), and samples were resuspended in SDS sample buffer (Thermo Scientific). Samples were boiled and electrophoresed by SDS-PAGE. Proteins were then transferred to nitrocellulose membranes (Whatman). The membranes were blocked with TBST (25 mM Tris-HCl, pH 7.5, 150 mM NaCl, 0.05% Tween 20) containing 5% nonfat dried milk or 5% BSA and probed overnight with primary antibodies, followed by 2 h incubation with secondary antibodies coupled to peroxidase. Blots were developed by using enhanced chemiluminescence.

RT-qPCR analysis—RT-qPCR analysis was performed as described previously.[59] Total RNA was isolated using the RNeasy mini kit (Qiagen), and the first-strand cDNA was prepared using superscript III first-strand synthesis supermix kit (Invitrogen) according to the manufacturers' protocol. qPCR was performed using QuantiTech SYBR green PCR kit (Qiagen) on CFX96 real-time PCR (Bio-Rad) and ABI ViiA7 real-time PCR systems (Life Technologies). Pre-designed KiCqStart SYBR Green Primers were purchased from Sigma, and melting curve analysis was performed at the end of PCR.

RNA sequencing and data analysis—RNA extraction, RNA sequencing, and data analysis were performed at Genewiz. Briefly, after investigating the quality of the raw data, sequence reads were trimmed to remove possible adapter sequences and nucleotides with poor quality using Trimmomatic v.0.36. The trimmed reads were mapped to the reference genome available on ENSEMBL using the STAR aligner v.2.5.2b. The STAR aligner uses a splice aligner that detects splice junctions and incorporates them to help align the entire read sequences. BAM files were generated as a result of this step. Unique gene hit counts were

calculated by using feature Counts from the Subread package v.1.5.2. Only unique reads that fell within exon regions were counted. After extraction of gene hit counts, the gene hit counts table was used for downstream differential expression analysis. Using DESeq2, a comparison of gene expression between the groups of samples was performed. The Wald test was used to generate p values and Log_2 (fold changes). Genes with adjusted p values <0.05 and absolute log_2 (fold changes) > 1 were called as differentially expressed genes for each comparison. A gene ontology analysis was performed on the statistically significant set of genes by implementing the software GeneSCF. The mgi GO list was used to cluster the set of genes based on their biological process and determine their statistical significance. A PCA analysis was performed using the "plotPCA" function within the DESeq2 R package. The plot shows the samples in a 2D plane spanned by their first two principal components. The top 500 genes, selected by highest row variance, were used to generate the plot.

Tandem mass tag (TMT) mass spectrometry

Sample preparation for tandem mass tag (TMT) mass spectrometry: Samples for protein and "mini-phos" analysis were prepared as previously described.[60,61] Following lysis, protein precipitation, reduction/alkylation and digestion, peptides were quantified by micro-BCA assay and 300μg of peptide per sample were labeled with TMTPro reagents (Thermo-Fisher) for 2 h at room temperature. Labeling reactions were quenched with 0.5% hydroxylamine and acidified with TFA. Acidified peptides were combined and desalted by Sep-Pak (Waters). "mini-phos" enrichment was performed as previously described.[60] Peptides from the flow-through were further fractionated for full proteome analysis.

Basic pH reversed-phase separation (BPRP) of TMT-labeled peptides: TMT-labeled peptides were solubilized in 5% ACN/10 mM ammonium bicarbonate, pH 8.0, and 300 μg of TMT-labeled peptides were separated by an Agilent 300 Extend C18 column (3.5 μm particles, 4.6 mm ID and 250 mm in length). An Agilent 1260 binary pump coupled with a photodiode array (PDA) detector (Thermo Scientific) was used to separate the peptides. A 45-min linear gradient from 10% to 40% acetonitrile in 10 mM ammonium bicarbonate pH 8.0 (flow rate of 0.6 mL/min) separated the peptide mixtures into a total of 96 fractions (36 s). A total of 96 Fractions were consolidated into 24 samples in a checkerboard fashion, acidified with 20 μL of 10% formic acid, and vacuum dried to completion. Each sample was desalted via Stage Tips and re-dissolved in 5% FA/5% ACN for LC-MS3 analysis.

Liquid chromatography separation and tandem mass spectrometry (LC-MS3): Proteome data were collected on an Orbitrap Eclipse mass spectrometer (ThermoFisher Scientific) coupled to a Proxeon EASY-nLC 1200 LC pump (ThermoFisher Scientific). Fractionated peptides were separated using a 120 min gradient at 500 nL/min on a 35 cm column (i.d. 100 μm, Accucore, 2.6 μm, 150 Å) packed in-house. High-field asymmetric-waveform ion mobility spectrometry (FAIMS) was enabled during data acquisition with compensation voltages set as −40, −60, and −80 V.[62] MS1 data were collected in the Orbitrap (60,000 resolution; maximum injection time 50 ms; AGC 4 × 105). Charge states between 2 and 5 were required for MS2 analysis, and a 120 s dynamic exclusion window was used. Cycle time was set at 1.2 s. MS2 scans were performed in the ion trap with CID fragmentation (isolation window 0.5 Da; Turbo; NCE 35%;

maximum injection time 35 ms; AGC 1×104). An online real-time search algorithm (Orbiter) was used to trigger MS3 scans for quantification.[63] MS3 scans were collected in the Orbitrap using a resolution of 50,000, NCE of 45%, maximum injection time of 150 ms, and AGC of 1.5×105. The close-out was set at two peptides per protein per fraction.[63] Phosphorylated peptides were separated using a 120 min gradient with FAIMS enabled during data acquisition with compensation voltages set as −40, −60, and −80 V for the first shot and −45 and −65 V for the second shot.[62] MS1 data were collected in the Orbitrap (120,000 resolution; maximum injection time 50 ms; AGC 4×105). Charge states between 2 and 5 were required for MS2 analysis, and a 90 s dynamic exclusion window was used. Cycle time was set at 1.25 s. MS2 scans were performed in the Orbitrap with HCD fragmentation (isolation window 0.5 Da; 50,000 resolution; NCE 36%; maximum injection time 250 ms; AGC 1.5×105).

TMT and phosphorylation data analysis: Raw files were converted to mzXML, and monoisotopic peaks were re-assigned using Monocle.[64] Searches were performed using the Comet search algorithm against a mouse database downloaded from Uniprot in May 2021. We used a 50 ppm precursor ion tolerance and 0.9 Da product ion tolerance for MS2 scans collected in the ion trap and 0.02 Da product ion tolerance for MS2 scans collected in the Orbitrap. TMTpro on lysine residues and peptide N-termini (+304.2071 Da) and carbamidomethylation of cysteine residues (+57.0215 Da) were set as static modifications, while oxidation of methionine residues (+15.9949 Da) was set as a variable modification. For phosphorylated peptide analysis, +79.9663 Da was set as a variable modification on serine, threonine, and tyrosine residues. Each run was filtered separately to 1% False Discovery Rate (FDR) on the peptide-spectrum match (PSM) level. Then proteins were filtered to the target 1% FDR level across the entire combined dataset. Phosphorylation site localization was determined using the AScore algorithm.[65] For reporter ion quantification, a 0.003 Da window around the theoretical m/z of each reporter ion was scanned, and the most intense m/z was used. Reporter ion intensities were adjusted to correct for isotopic impurities of the different TMTpro reagents according to manufacturer specifications. Peptides were filtered to include only those with a summed signal-to-noise (SN) 100 across all TMT channels. An extra filter of an isolation specificity ("isolation purity") of at least 0.5 in the MS1 isolation window was applied for the phosphorylated peptide analysis. For each protein or phosphorylation site, the filtered peptide TMTpro SN values were summed to generate protein or phosphorylation site quantification values. To control for different total protein loading within a TMTpro experiment, the summed protein quantities of each channel were adjusted to be equal within the experiment. The functional enrichment analysis using TMT data was performed by Metascape.

RNA-binding protein immunoprecipitation—RNA-binding protein immunoprecipitation (RIP) was performed using an imprint RIP kit (Sigma) according to the manufacturer's protocol with some modifications. Briefly, stable cells infected with vector control or HA-eIF3D plasmids treated with or without an mTOR inhibitor were lysed. Immunoprecipitation was performed using anti-HA magnetic beads (Thermo Scientific). After washing with RIP wash buffer five times, proteins and DNA were removed by

proteinase K and DNaseI, respectively. RNA was collected by acidic phenol extraction followed by precipitation with ethanol, sodium acetate, and GlycoBlue.

Nascent protein synthesis assay—Nascent protein synthesis assay was performed using Click-iT AHA (l-Azidohomoalanine), Tetramethylrhodamine (TAMRA) Alkyne, and Click-iT protein reaction buffer kit according to the manufacturer (Invitrogen)'s protocol. Briefly, cells were incubated with AHA in methionine-free media. Cells were lysed, and the lysate was incubated with TAMRA in a click-iT protein reaction buffer. After protein collection with methanol/chloroform precipitation and wash with methanol, protein gel electrophoresis was performed.

Mass spectrometry analysis for eIF3D interacting molecule identification—Cells stably expressing HA-eIF3D were lysed, and immunoprecipitation with anti-HA magnets (Thermo Scientific) was performed according to the manufacturer's protocol. The beads were washed, and proteins were eluted with HA peptide (Pierce). Elute was mixed with 100% TCA (final 20%), vortexed, and incubated on ice for 25 min. After centrifugation at 14,000 rpm at 4°C for 25 min, the supernatant was removed. The clear pellet was washed with 10% TCA one time and ice-cold acetone three times with centrifugation at 14,000 rpm at 4°C for 25 min and removal of supernatant each time. Pellet was air-dried at room temperature. For mass spectrometry analysis, the protein pellets were re-suspended in 50 μL of 8 M urea, 50 mM ammonium bicarbonate (ambic), then reduced and alkylated with dithiothreitol and iodoacetamide. They were diluted to 2 M urea with 50 mM ambic, digested with LysC (10 ng/μL, Wako Chemicals) overnight, then diluted to 1 M urea and digested with Trypsin (10 ng/μL, Promega). Peptides were desalted on C18 STAGE tips [PMID: 12585499], eluted, and dried in sample vials. Dry peptides were resuspended in 5% FA and separated using an Easy nLC-1000 HPLC (Thermo) on a self-packed 40 cm, 75 μm inside diameter, column packed with 1.8 μm, C18 resin (SEPAX) using a gradient of 5–26% buffer B (95% ACN, 0.1% FA) at a flow rate of 350 nL/min for 75 min. Peptides were analyzed on a Thermo Orbitrap Fusion mass spectrometer equipped with a FAIMS Pro ion mobility cell. The FAIMS was used to cycle through five different compensation voltages (CV: −40, −50, −60, −70, −80). We collected one precursor MS1 scan for each CV at 120K resolution, with 4e5 AGC target, and a 50 ms max ion accumulation time. For each MS1, peptides were fragmented using HCD with a normalized collision energy of 28% and scanned in the ion trap using the "rapid" scan rate with AGC = 1e4 and max ion accumulation = 35 ms. Dynamic exclusion was enabled to exclude ions that had already been selected for MS/MS in the previous 45 s. Ions with a charge of +1 and those whose charge state could not be assigned were also excluded. MS2 spectra were searched using COMET (version 2020.01 rev. 4) against a composite database containing the canonical Swiss-Prot reviewed mouse protein sequences (17,009 www.uniprot.org) and their reversed complement, using the following parameters: a precursor mass tolerance of ±25ppm; 1.0 Da product ion mass tolerance; tryptic digestion; up to two missed cleavages; static modifications of carbamidomethylation on cysteine (+57.0214); a dynamic modification of methionine oxidation (+15.9949). Peptide spectral matches (PSMs) were filtered to 1% FDR using the target-decoy strategy[66] combined with linear discriminant analysis (LDA)[67] using several different parameters, including the Comet Expect score, ΔExpect, precursor mass

error, and observed ion charge state. The data were further filtered to control protein level FDRs. Peptides were combined and assembled into proteins. Protein scores were derived from the product of LDA peptide probabilities. The FDR of the remaining peptides fell dramatically after protein filtering. We required all peptides to have a signal-to-noise ratio (SN) $\geqq 5$. Protein ratios were calculated as the $\log_2$ ratio of the total SN of all experimental sample peptide values over that for IgG control sample peptides.

Migration and invasion assay—Cell migration and invasion assays were performed as described previously.[26] Cells were pre-incubated with or without mTOR inhibitors for 48 h in 10 cm plates. Cells were then trypsinized and collected. Media were aspirated, and cells were resuspended in serum-free media. For migration assays, media with 10% FBS was added to the bottom chamber of the cell culture inserts. Cells ($5 \times 10^4/200$ μL) were added to the top chamber of cell culture inserts (8 μm pore size) in a 24-well companion plate. Specifically, cells incubated in 10 cm plates in the absence of mTOR inhibitors were used as a control for migration assay that was performed with DMSO (control for inhibitors) in the upper and lower chamber. Cells grown in 10 cm plates in the presence of mTOR inhibitors were used with mTOR inhibitors and other inhibitors in the upper and lower chamber for migration assay in the cell culture inserts. After 12-h incubation, the cells that migrated to the lower surface of the membrane were fixed with methanol and stained with 0.2% crystal violet in 2% ethanol. The number of migrated cells was quantified by counting random distinct fields using a light microscope. For cell invasion assays, BD BioCoat invasion chambers coated with Matrigel were used. Invasion chambers were prepared according to the manufacturer's specifications, and assays were performed as described in migration assays, except the assay was performed for 23 h.

Image analysis—Band intensities from Western blot analysis were determined by GelQuantNet V1.8.2. Statistical analysis was performed using GraphPrism 9 and Microsoft Excel.

QUANTIFICATION AND STATISTICAL ANALYSIS

Statistical analysis was performed using GraphPad Prism 9 and Microsoft Excel. Data were presented as means and error bars representing standard deviations. Statistical significance was defined as a p value of 0.05 or lower, which was assessed by the unpaired t test. Statistical details of experiments, including numbers of biological or technical replicates, are described in each figure legend.

Supplementary Material

Refer to Web version on PubMed Central for supplementary material.

ACKNOWLEDGMENTS

REFERENCES

1. Hipp MS, Kasturi P, and Hartl FU (2019). The proteostasis network and its decline in ageing. Nat. Rev. Mol. Cell Biol 20, 421–435. 10.1038/s41580-019-0101-y. [PubMed: 30733602]

2. Ottens F, Franz A, and Hoppe T (2021). Build-UPS and break-downs: metabolism impacts on proteostasis and aging. Cell Death Differ. 28, 505–521. 10.1038/s41418-020-00682-y. [PubMed: 33398091]

3. Szwed A, Kim E, and Jacinto E (2021). Regulation and metabolic functions of mTORC1 and mTORC2. Physiol. Rev 101, 1371–1426. 10.1152/physrev.00026.2020. [PubMed: 33599151]

4. Jackson RJ, Hellen CUT, and Pestova TV (2010). The mechanism of eukaryotic translation initiation and principles of its regulation. Nat. Rev. Mol. Cell Biol 11, 113–127. 10.1038/nrm2838. [PubMed: 20094052]

5. Pelletier J, and Sonenberg N (2019). The Organizing Principles of Eukaryotic Ribosome Recruitment. Annu. Rev. Biochem 88, 307–335. 10.1146/annurev-biochem-013118-111042. [PubMed: 31220979]

6. Musa J, Orth MF, Dallmayer M, Baldauf M, Pardo C, Rotblat B, Kirchner T, Leprivier G, and Grünewald TGP (2016). Eukaryotic initiation factor 4E-binding protein 1 (4E-BP1): a master regulator of mRNA translation involved in tumorigenesis. Oncogene 35, 4675–4688. 10.1038/onc.2015.515. [PubMed: 26829052]

7. Roux PP, and Topisirovic I (2018). Signaling Pathways Involved in the Regulation of mRNA Translation. Mol. Cell Biol 38, e00070–18. 10.1128/MCB.00070-18. [PubMed: 29610153]

8. Bhat M, Robichaud N, Hulea L, Sonenberg N, Pelletier J, and Topisirovic I (2015). Targeting the translation machinery in cancer. Nat. Rev. Drug Discov 14, 261–278. 10.1038/nrd4505. [PubMed: 25743081]

9. Hao P, Yu J, Ward R, Liu Y, Hao Q, An S, and Xu T (2020). Eukaryotic translation initiation factors as promising targets in cancer therapy. Cell Commun. Signal 18, 175. 10.1186/s12964-020-00607-9. [PubMed: 33148274]

10. Holz MK, Ballif BA, Gygi SP, and Blenis J (2005). mTOR and S6K1 mediate assembly of the translation preinitiation complex through dynamic protein interchange and ordered phosphorylation events. Cell 123, 569–580. 10.1016/j.cell.2005.10.024. [PubMed: 16286006]

11. Dorrello NV, Peschiaroli A, Guardavaccaro D, Colburn NH, Sherman NE, and Pagano M (2006). S6K1- and betaTRCP-mediated degradation of PDCD4 promotes protein translation and cell growth. Science 314, 467–471. 10.1126/science.1130276. [PubMed: 17053147]

12. Su KH, and Dai C (2017). mTORC1 senses stresses: Coupling stress to proteostasis. Bioessays 39, 1600268. 10.1002/bies.201600268.

13. Zhang Y, Nicholatos J, Dreier JR, Ricoult SJH, Widenmaier SB, Hotamisligil GS, Kwiatkowski DJ, and Manning BD (2014). Coordinated regulation of protein synthesis and degradation by mTORC1. Nature 513, 440–443. 10.1038/nature13492. [PubMed: 25043031]

14. Zhao J, Zhai B, Gygi SP, and Goldberg AL (2015). mTOR inhibition activates overall protein degradation by the ubiquitin proteasome system as well as by autophagy. Proc. Natl. Acad. Sci. USA 112, 15790–15797. 10.1073/pnas.1521919112. [PubMed: 26669439]

15. Liu GY, and Sabatini DM (2020). mTOR at the nexus of nutrition, growth, ageing and disease. Nat. Rev. Mol. Cell Biol 21, 183–203. 10.1038/s41580-019-0199-y. [PubMed: 31937935]

16. Aylett CHS, Sauer E, Imseng S, Boehringer D, Hall MN, Ban N, and Maier T (2016). Architecture of human mTOR complex 1. Science 351, 48–52. 10.1126/science.aaa3870. [PubMed: 26678875]

17. Thoreen CC, Kang SA, Chang JW, Liu Q, Zhang J, Gao Y, Reichling LJ, Sim T, Sabatini DM, and Gray NS (2009). An ATP-competitive mammalian target of rapamycin inhibitor reveals rapamycin-resistant functions of mTORC1. J. Biol. Chem 284, 8023–8032. 10.1074/jbc.M900301200. [PubMed: 19150980]

18. Feldman ME, Apsel B, Uotila A, Loewith R, Knight ZA, Ruggero D, and Shokat KM (2009). Active-site inhibitors of mTOR target rapamycin-resistant outputs of mTORC1 and mTORC2. PLoS Biol. 7, e38. 10.1371/journal.pbio.1000038. [PubMed: 19209957]

19. Liu Q, Chang JW, Wang J, Kang SA, Thoreen CC, Markhard A, Hur W, Zhang J, Sim T, Sabatini DM, and Gray NS (2010). Discovery of 1-(4-(4-propionylpiperazin-1-yl)-3-

(trifluoromethyl)phenyl)-9-(quinolin-3-yl)benz o[h] [1,6]naphthyridin-2(1H)-one as a highly potent, selective mammalian target of rapamycin (mTOR) inhibitor for the treatment of cancer. J. Med. Chem 53, 7146–7155. 10.1021/jm101144f. [PubMed: 20860370]

20. Rodrik-Outmezguine VS, Okaniwa M, Yao Z, Novotny CJ, McWhirter C, Banaji A, Won H, Wong W, Berger M, de Stanchina E, et al. (2016). Overcoming mTOR resistance mutations with a new-generation mTOR inhibitor. Nature 534, 272–276. 10.1038/nature17963. [PubMed: 27279227]

21. Henske EP, Jó wiak S, Kingswood JC, Sampson JR, and Thiele EA (2016). Tuberous sclerosis complex. Nat. Rev. Dis. Prim 2, 16035. 10.1038/nrdp.2016.35. [PubMed: 27226234]

22. Dowling RJO, Topisirovic I, Alain T, Bidinosti M, Fonseca BD, Petroulakis E, Wang X, Larsson O, Selvaraj A, Liu Y, et al. (2010). mTORC1-mediated cell proliferation, but not cell growth, controlled by the 4E-BPs. Science 328, 1172–1176. 10.1126/science.1187532. [PubMed: 20508131]

23. Esposito DL, Li Y, Cama A, and Quon MJ (2001). Tyr(612) and Tyr(632) in human insulin receptor substrate-1 are important for full activation of insulin-stimulated phosphatidylinositol 3-kinase activity and translocation of GLUT4 in adipose cells. Endocrinology 142, 2833–2840. 10.1210/endo.142.7.8283. [PubMed: 11416002]

24. Um SH, Frigerio F, Watanabe M, Picard F, Joaquin M, Sticker M, Fumagalli S, Allegrini PR, Kozma SC, Auwerx J, and Thomas G (2004). Absence of S6K1 protects against age- and diet-induced obesity while enhancing insulin sensitivity. Nature 431, 200–205. 10.1038/nature02866. [PubMed: 15306821]

25. Rodrik-Outmezguine VS, Chandarlapaty S, Pagano NC, Poulikakos PI, Scaltriti M, Moskatel E, Baselga J, Guichard S, and Rosen N (2011). mTOR kinase inhibition causes feedback-dependent biphasic regulation of AKT signaling. Cancer Discov. 1, 248–259. 10.1158/2159-8290.CD-11-0085. [PubMed: 22140653]

26. Yoon SO, Shin S, Karreth FA, Buel GR, Jedrychowski MP, Plas DR, Dedhar S, Gygi SP, Roux PP, Dephoure N, and Blenis J (2017). Focal Adhesion- and IGF1R-Dependent Survival and Migratory Pathways Mediate Tumor Resistance to mTORC1/2 Inhibition. Mol. Cell 67, 512–527.e4. 10.1016/j.molcel.2017.06.033. [PubMed: 28757207]

27. Hua H, Kong Q, Yin J, Zhang J, and Jiang Y (2020). Insulin-like growth factor receptor signaling in tumorigenesis and drug resistance: a challenge for cancer therapy. J. Hematol. Oncol 13, 64. 10.1186/s13045-020-00904-3. [PubMed: 32493414]

28. Kang S, Tanaka T, Narazaki M, and Kishimoto T (2019). Targeting Interleukin-6 Signaling in Clinic. Immunity 50, 1007–1023. 10.1016/j.immuni.2019.03.026. [PubMed: 30995492]

29. Johnson DE, O'Keefe RA, and Grandis JR (2018). Targeting the IL-6/JAK/STAT3 signalling axis in cancer. Nat. Rev. Clin. Oncol 15, 234–248. 10.1038/nrclinonc.2018.8. [PubMed: 29405201]

30. Shah OJ, Wang Z, and Hunter T (2004). Inappropriate activation of the TSC/Rheb/mTOR/S6K cassette induces IRS1/2 depletion, insulin resistance, and cell survival deficiencies. Curr. Biol 14, 1650–1656. 10.1016/j.cub.2004.08.026. [PubMed: 15380067]

31. Briaud I, Dickson LM, Lingohr MK, McCuaig JF, Lawrence JC, and Rhodes CJ (2005). Insulin receptor substrate-2 proteasomal degradation mediated by a mammalian target of rapamycin (mTOR)-induced negative feedback down-regulates protein kinase B-mediated signaling pathway in beta-cells. J. Biol. Chem 280, 2282–2293. 10.1074/jbc.M412179200. [PubMed: 15537654]

32. Yu Y, Yoon SO, Poulogiannis G, Yang Q, Ma XM, Villén J, Kubica N, Hoffman GR, Cantley LC, Gygi SP, and Blenis J (2011). Phosphoproteomic analysis identifies Grb10 as an mTORC1 substrate that negatively regulates insulin signaling. Science 332, 1322–1326. 10.1126/science.1199484. [PubMed: 21659605]

33. Uniacke J, Holterman CE, Lachance G, Franovic A, Jacob MD, Fabian MR, Payette J, Holcik M, Pause A, and Lee S (2012). An oxygen-regulated switch in the protein synthesis machinery. Nature 486, 126–129. 10.1038/nature11055. [PubMed: 22678294]

34. Genuth NR, and Barna M (2018). Heterogeneity and specialized functions of translation machinery: from genes to organisms. Nat. Rev. Genet 19, 431–452. 10.1038/s41576-018-0008-z. [PubMed: 29725087]

35. Ho JJD, and Lee S (2016).A Cap for Every Occasion: Alternative eIF4F Complexes. Trends Biochem. Sci 41, 821–823. 10.1016/j.tibs.2016.05.009. [PubMed: 27283511]

36. Valášek LS, Zeman J, Wagner S, Beznosková P, Pavlíková Z, Mohammad MP, Hronová V, Herrmannová A, Hashem Y, and Gunišová S (2017). Embraced by eIF3: structural and functional insights into the roles of eIF3 across the translation cycle. Nucleic Acids Res. 45, 10948–10968. 10.1093/nar/gkx805. [PubMed: 28981723]

37. Hentze MW, Castello A, Schwarzl T, and Preiss T (2018). A brave new world of RNA-binding proteins. Nat. Rev. Mol. Cell Biol 19, 327–341. 10.1038/nrm.2017.130. [PubMed: 29339797]

38. Thomas SJ, Snowden JA, Zeidler MP, and Danson SJ (2015). The role of JAK/STAT signalling in the pathogenesis, prognosis and treatment of solid tumours. Br. J. Cancer 113, 365–371. 10.1038/bjc.2015.233. [PubMed: 26151455]

39. Hershey JWB, Sonenberg N, and Mathews MB (2019). Principles of Translational Control. Cold Spring Harbor Perspect. Biol 11, a032607. 10.1101/cshperspect.a032607.

40. Morita M, Ler LW, Fabian MR, Siddiqui N, Mullin M, Henderson VC, Alain T, Fonseca BD, Karashchuk G, Bennett CF, et al. (2012). A novel 4EHP-GIGYF2 translational repressor complex is essential for mammalian development. Mol. Cell Biol 32, 3585–3593. 10.1128/MCB.00455-12. [PubMed: 22751931]

41. David M, Olender T, Mizrahi O, Weingarten-Gabbay S, Friedlander G, Meril S, Goldberg N, Savidor A, Levin Y, Salomon V, et al. (2022). DAP5 drives translation of specific mRNA targets with upstream ORFs in human embryonic stem cells. RNA 28, 1325–1336. 10.1261/rna.079194.122. [PubMed: 35961752]

42. de la Parra C, Ernlund A, Alard A, Ruggles K, Ueberheide B, and Schneider RJ (2018). A widespread alternate form of cap-dependent mRNA translation initiation. Nat. Commun 9, 3068. 10.1038/s41467-018-05539-0. [PubMed: 30076308]

43. Cate JHD (2017). Human eIF3: from 'blobology' to biological insight. Philos. Trans. R. Soc. Lond. B Biol. Sci 372, 20160176. 10.1098/rstb.2016.0176. [PubMed: 28138064]

44. Wagner S, Herrmannová A, Malík R, Peclinovská L, and Valášek LS (2014). Functional and biochemical characterization of human eukaryotic translation initiation factor 3 in living cells. Mol. Cell Biol 34, 3041–3052. 10.1128/MCB.00663-14. [PubMed: 24912683]

45. Chu J, Cargnello M, Topisirovic I, and Pelletier J (2016). Translation Initiation Factors: Reprogramming Protein Synthesis in Cancer. Trends Cell Biol. 26, 918–933. 10.1016/j.tcb.2016.06.005. [PubMed: 27426745]

46. Herrmannová A, Prilepskaja T, Wagner S, Šikrová D, Zeman J, Poncová K, and Valášek LS (2020). Adapted formaldehyde gradient cross-linking protocol implicates human eIF3d and eIF3c, k and l subunits in the 43S and 48S pre-initiation complex assembly, respectively. Nucleic Acids Res. 48, 1969–1984. 10.1093/nar/gkz1185. [PubMed: 31863585]

47. Wagner S, Herrmannová A, Šikrová D, and Valášek LS (2016). Human eIF3b and eIF3a serve as the nucleation core for the assembly of eIF3 into two interconnected modules: the yeast-like core and the octamer. Nucleic Acids Res. 44, 10772–10788. 10.1093/nar/gkw972. [PubMed: 27924037]

48. Lee AS, Kranzusch PJ, Doudna JA, and Cate JHD (2016). eIF3d is an mRNA cap-binding protein that is required for specialized translation initiation. Nature 536, 96–99. 10.1038/nature18954. [PubMed: 27462815]

49. Guan BJ, van Hoef V, Jobava R, Elroy-Stein O, Valasek LS, Cargnello M, Gao XH, Krokowski D, Merrick WC, Kimball SR, et al. (2017). A Unique ISR Program Determines Cellular Responses to Chronic Stress. Mol. Cell 68, 885–900.e6. 10.1016/j.molcel.2017.11.007. [PubMed: 29220654]

50. Volta V, Pérez-Baos S, de la Parra C, Katsara O, Ernlund A, Dornbaum S, and Schneider RJ (2021). A DAP5/eIF3d alternate mRNA translation mechanism promotes differentiation and immune suppression by human regulatory T cells. Nat. Commun 12, 6979. 10.1038/s41467-021-27087-w. [PubMed: 34848685]

51. Lamper AM, Fleming RH, Ladd KM, and Lee ASY (2020). A phosphorylation-regulated eIF3d translation switch mediates cellular adaptation to metabolic stress. Science 370, 853–856. 10.1126/science.abb0993. [PubMed: 33184215]

52. Liu Y, Beyer A, and Aebersold R (2016). On the Dependency of Cellular Protein Levels on mRNA Abundance. Cell 165, 535–550. 10.1016/j.cell.2016.03.014. [PubMed: 27104977]

53. Vogel C, and Marcotte EM (2012). Insights into the regulation of protein abundance from proteomic and transcriptomic analyses. Nat. Rev. Genet 13, 227–232. 10.1038/nrg3185. [PubMed: 22411467]

54. Sriram A, Bohlen J, and Teleman AA (2018). Translation acrobatics: how cancer cells exploit alternate modes of translational initiation. EMBO Rep. 19, e45947. 10.15252/embr.201845947. [PubMed: 30224410]

55. Kusnadi EP, Timpone C, Topisirovic I, Larsson O, and Furic L (2022). Regulation of gene expression via translational buffering. Biochim. Biophys. Acta Mol. Cell Res 1869, 119140. 10.1016/j.bbamcr.2021.119140. [PubMed: 34599983]

56. Dominguez D, Freese P, Alexis MS, Su A, Hochman M, Palden T, Bazile C, Lambert NJ, Van Nostrand EL, Pratt GA, et al. (2018). Sequence, Structure, and Context Preferences of Human RNA Binding Proteins. Mol. Cell 70, 854–867.e9. 10.1016/j.molcel.2018.05.001. [PubMed: 29883606]

57. O'Shea JJ, Schwartz DM, Villarino AV, Gadina M, McInnes IB, and Laurence A (2015). The JAK-STAT pathway: impact on human disease and therapeutic intervention. Annu. Rev. Med 66, 311–328. 10.1146/annurev-med-051113-024537. [PubMed: 25587654]

58. Jewer M, Lee L, Leibovitch M, Zhang G, Liu J, Findlay SD, Vincent KM, Tandoc K, Dieters-Castator D, Quail DF, et al. (2020). Translational control of breast cancer plasticity. Nat. Commun 11, 2498. 10.1038/s41467-020-16352-z. [PubMed: 32427827]

59. Shin S, Buel GR, Wolgamott L, Plas DR, Asara JM, Blenis J, and Yoon SO (2015). ERK2 Mediates Metabolic Stress Response to Regulate Cell Fate. Mol. Cell 59, 382–398, S1097-2765(15)00492-X [pii]. 10.1016/j.molcel.2015.06.020. [PubMed: 26190261]

60. Navarrete-Perea J, Yu Q, Gygi SP, and Paulo JA (2018). Streamlined Tandem Mass Tag (SL-TMT) Protocol: An Efficient Strategy for Quantitative (Phospho)proteome Profiling Using Tandem Mass Tag-Synchronous Precursor Selection-MS3. J. Proteome Res 17, 2226–2236. 10.1021/acs.jproteome.8b00217. [PubMed: 29734811]

61. Li J, Cai Z, Bomgarden RD, Pike I, Kuhn K, Rogers JC, Roberts TM, Gygi SP, and Paulo JA (2021). TMTpro18plex: The Expanded and Complete Set of TMTpro Reagents for Sample Multiplexing. J. Proteome Res 20, 2964–2972. 10.1021/acs.jproteome.1c00168. [PubMed: 33900084]

62. Schweppe DK, Prasad S, Belford MW, Navarrete-Perea J, Bailey DJ, Huguet R, Jedrychowski MP, Rad R, McAlister G, Abbatiello SE, et al. (2019). Characterization and Optimization of Multiplexed Quantitative Analyses Using High-Field Asymmetric-Waveform Ion Mobility Mass Spectrometry. Anal. Chem 91, 4010–4016. 10.1021/acs.analchem.8b05399. [PubMed: 30672687]

63. Schweppe DK, Eng JK, Yu Q, Bailey D, Rad R, Navarrete-Perea J, Huttlin EL, Erickson BK, Paulo JA, and Gygi SP (2020). Full-Featured, Real-Time Database Searching Platform Enables Fast and Accurate Multiplexed Quantitative Proteomics. J. Proteome Res 19, 2026–2034. 10.1021/acs.jproteome.9b00860. [PubMed: 32126768]

64. Rad R, Li J, Mintseris J, O'Connell J, Gygi SP, and Schweppe DK (2021). Improved Monoisotopic Mass Estimation for Deeper Proteome Coverage. J. Proteome Res 20, 591–598. 10.1021/acs.jproteome.0c00563. [PubMed: 33190505]

65. Beausoleil SA, Villén J, Gerber SA, Rush J, and Gygi SP (2006). A probability-based approach for high-throughput protein phosphorylation analysis and site localization. Nat. Biotechnol 24, 1285–1292. 10.1038/nbt1240. [PubMed: 16964243]

66. Elias JE, and Gygi SP (2007). Target-decoy search strategy for increased confidence in large-scale protein identifications by mass spectrometry. Nat. Methods 4, 207–214. 10.1038/nmeth1019. [PubMed: 17327847]

67. Huttlin EL, Jedrychowski MP, Elias JE, Goswami T, Rad R, Beausoleil SA, Villén J, Haas W, Sowa ME, and Gygi SP (2010). A tissue-specific atlas of mouse protein phosphorylation and expression. Cell 143, 1174–1189. 10.1016/j.cell.2010.12.001. [PubMed: 21183079]

Highlights

- mTOR inhibition promotes eIF3D-dependent mRNA translation

- eIF3D cooperates with RNA-binding proteins for selective mRNA translation

- Insulin receptor and insulin-like growth factor 1 receptor are targets of eIF3D

- eIF3D-dependent protein upregulation promotes cancer cell migration and invasion
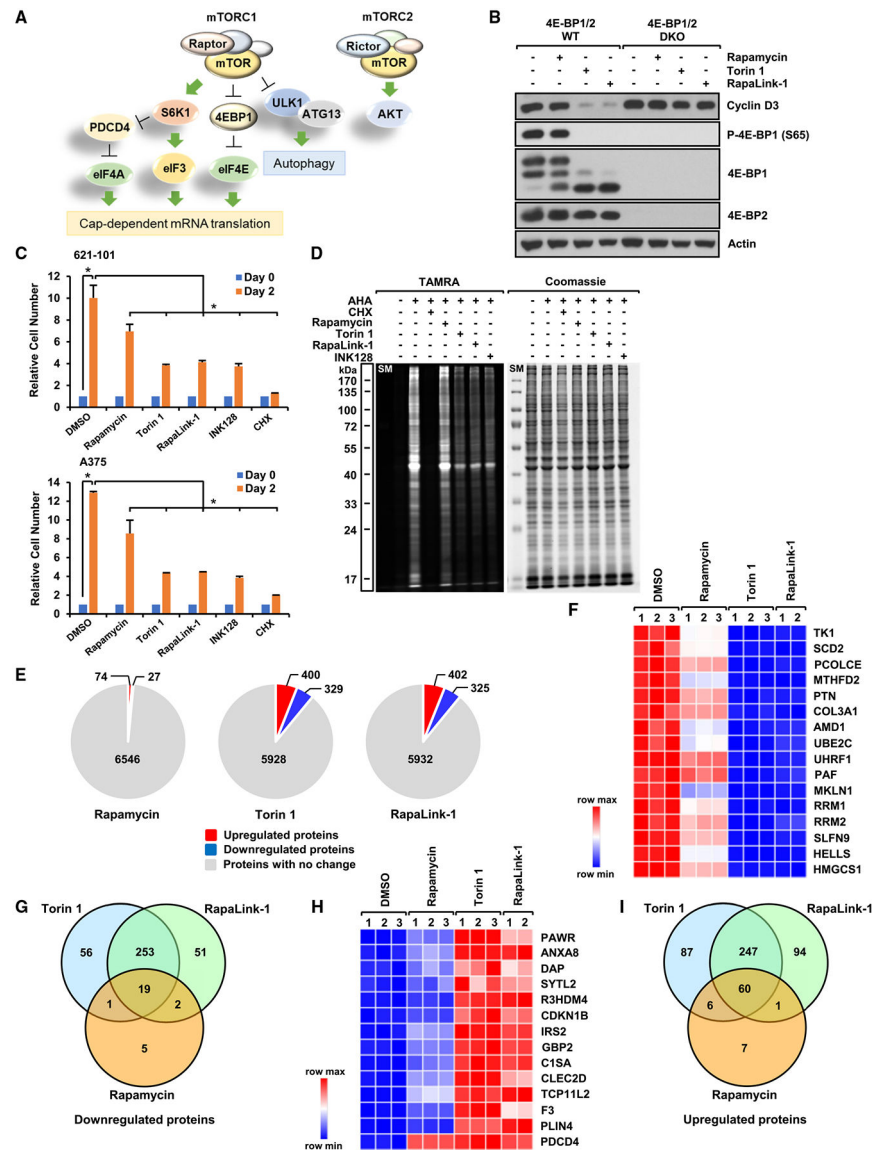
Figure 1. mTOR inhibition increases the expression of select proteins

(A) mTOR signaling pathways. (B) 4E-BP1/2 WT and double-KO (DKO) MEFs were treated with rapamycin (20 ng/mL), Torin1 (250 nM), and RapaLink-1 (10 nM) for 24 h, and immunoblot analysis was performed.

(C) Cells were treated with/without mTOR inhibitors, including INK128 (10 μM) and cycloheximide (CHX; 10 μg/mL), for 48 h, and cell numbers were counted. Data are the mean ± SD of three biological replicates. Statistical significance (*p < 0.05) was assessed by t test.

(D) The nascent protein synthesis rate was measured following mTOR inhibition.

(E–I) MEFs were treated with mTOR inhibitors for 24 h. Quantitative 11-plex mass spectrometry for complete protein profiling and data analysis was performed. (E) Statistical analysis was performed using data from three biological replicates for the control, rapamycin, and Torin1 treatments and two biological replicates for the RapaLink-1 treatment. The pie chart shows differentially ($Log_{1.5}$(fold change) >1 or < −1, false

discovery rate (FDR)-adjusted p < 0.05) and non-differentially expressed proteins. The heatmap and Venn diagram show (F and G) downregulated or (H and I) upregulated proteins.
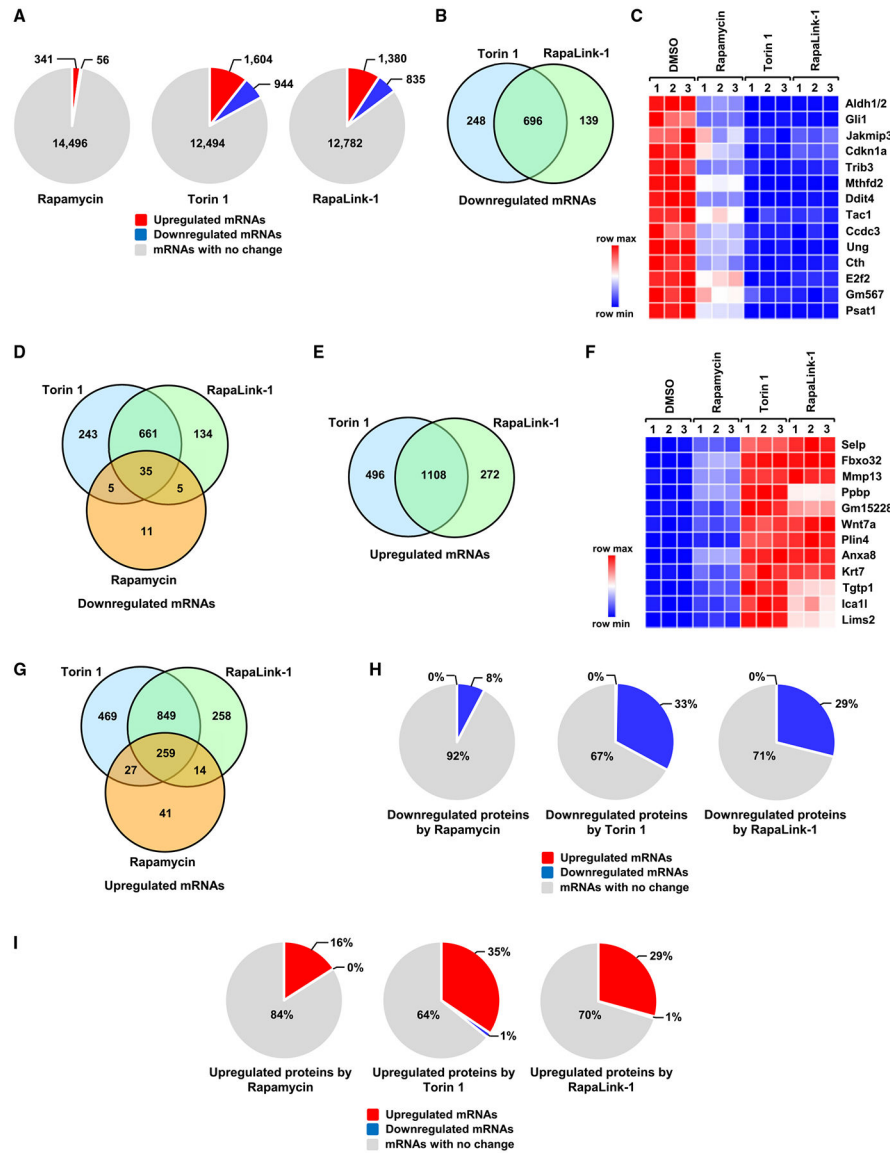
See also Figure S1.

Figure 2. mTOR-inhibition-mediated proteome change is independent of transcriptome change

(A–G) MEFs were treated with rapamycin (20 ng/mL), Torin1 (250 nM), and RapaLink-1 (10 nM) for 24 h. RNA sequencing and data analysis were performed. (A) Statistical analysis was performed using data from three biological replicates. The pie chart shows differentially ($\log_2$(fold change) > 1 or < −1, FDR-adjusted $p < 0.05$) and non-differentially expressed mRNAs. The Venn diagram and heatmap show (B–D) downregulated or (E–G) upregulated mRNAs.

(H and I) Data from proteome and transcriptome profiling were analyzed together. The pie charts show (H) downregulated or (I) upregulated proteins by mTOR inhibition and the levels of their corresponding mRNAs.
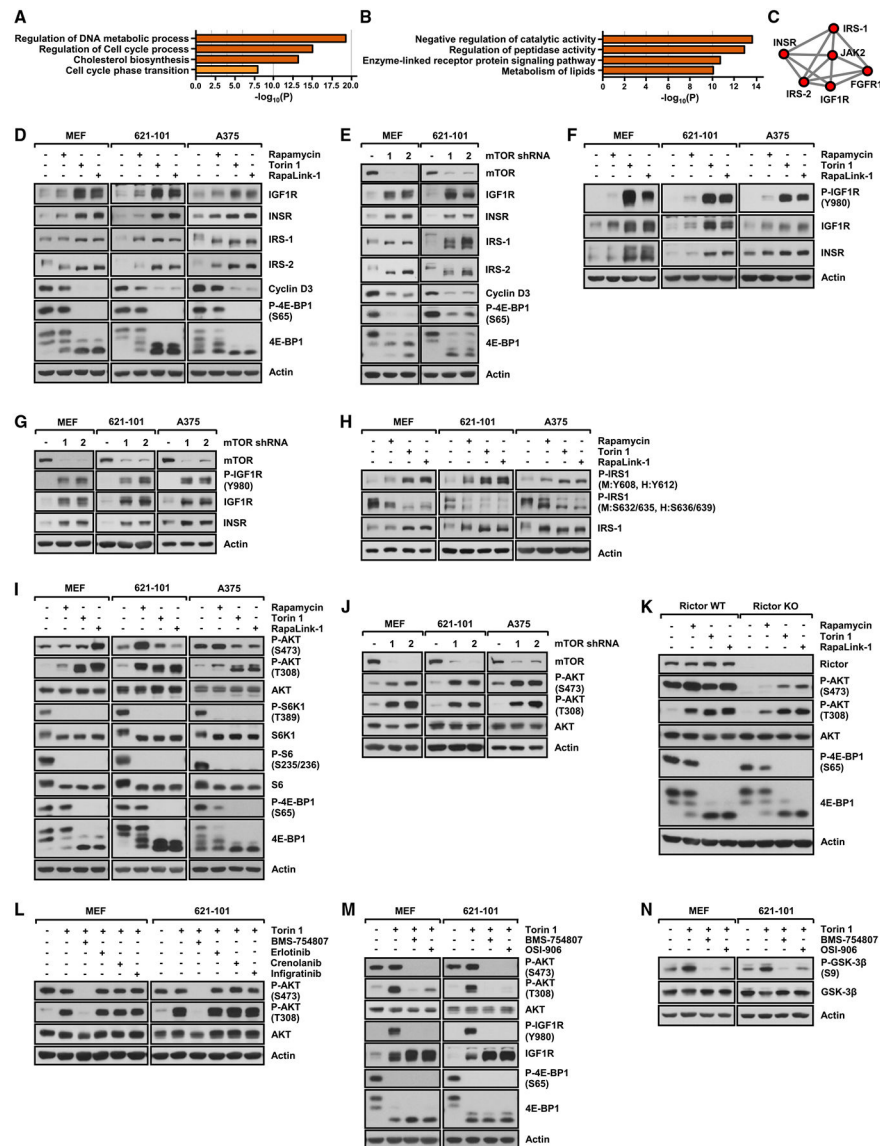
See also Figure S2.

Figure 3. mTOR inhibition activates INSR/IGF1R/IRS/AKT signaling

(A and B) Enrichment analysis with (A) downregulated and (B) upregulated proteins by both Torin1 and RapaLink-1.

(C) Interaction enrichment analysis with upregulated proteins by both Torin1 and RapaLink-1.

(D–J) Cells treated with/without rapamycin (20 ng/mL), Torin1 (250 nM), and RapaLink-1 (10 nM) for 24 h (D, F, H, and I) or stably knocked down cells with mTOR shRNAs (E, G, and J) were lysed, and immunoblot analysis was performed.

(K) Rictor WT or KO cells were treated with mTOR inhibitors for 24 h, and immunoblot analysis was performed.

(L–N) Cells were treated with Torin1 for 6 h, after which BMS754807 (10 μM, IGF1R inhibitor), erlotinib (5 μM, epidermal growth factor receptor(EGFR) inhibitor), crenolanib (0.5 μM, platelet-derived growth factor receptor (PDGFR) and FLT3 inhibitor), infigratinib

(0.5 μM, FGFR inhibitor), or OSI-906 (5 μM, IGF1R inhibitor) was treated for an additional 18 h in the presence of Torin1. Cells were lysed, and immunoblot analysis was performed. See also Figure S3.
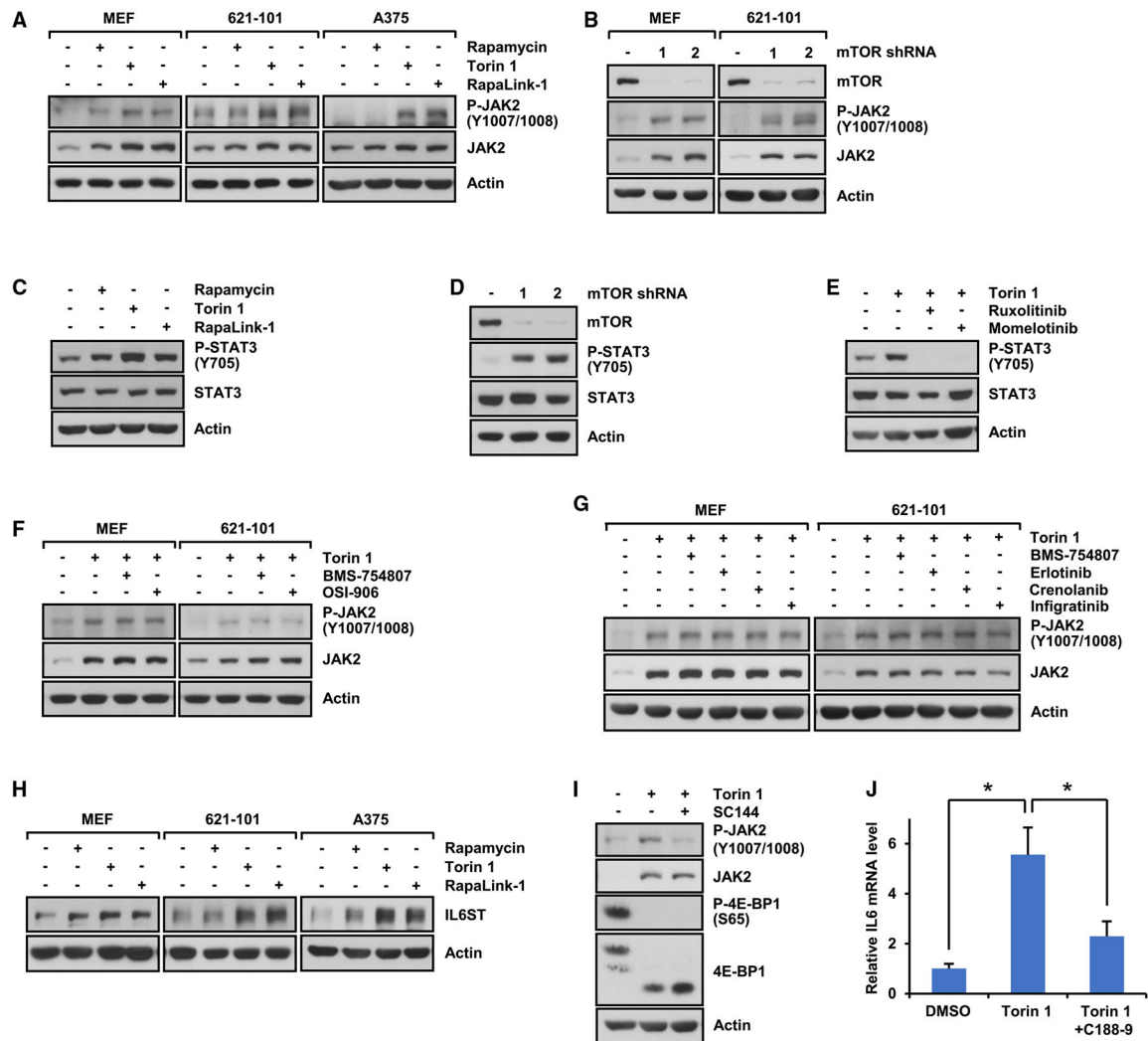
Figure 4. mTOR inhibition activates the JAK/STAT pathway

(A–D) Cells treated with/without rapamycin (20 ng/mL), Torin1 (250 nM), and RapaLink-1 (10 nM) for 24 h (A and C) or stable knockdown cells with mTOR shRNAs (B and D) were lysed, and immunoblot analysis was performed.

(E–G) Cells were treated with Torin1 for 6 h, after which (E) JAK1/2 inhibitors (ruxolitinib: 2.5 μM, momelotinib: 5 μM), (F) IGF1R inhibitors, or (G) RTK inhibitors as described in Figure 3 were treated for an additional 18 h in the presence of Torin1. Cells were lysed, and immunoblot analysis was performed.

(H) Cells were treated with/without mTOR inhibitors for 24 h, and immunoblot analysis was performed.

(I and J) Cells were treated with Torin1 for 6 h, after which (I) IL-6ST inhibitor (SC144: 10 μM) or (J) STAT3 inhibitor (C188-9: 10 μM) was treated for an additional 18 h in the presence of Torin1. (I and J) Immunoblot analysis (I) or qRT-PCR (J) was performed. Data are the mean ± SD of three technical replicates. Statistical significance (*p < 0.05) was assessed by t test.

See also Figure S4.
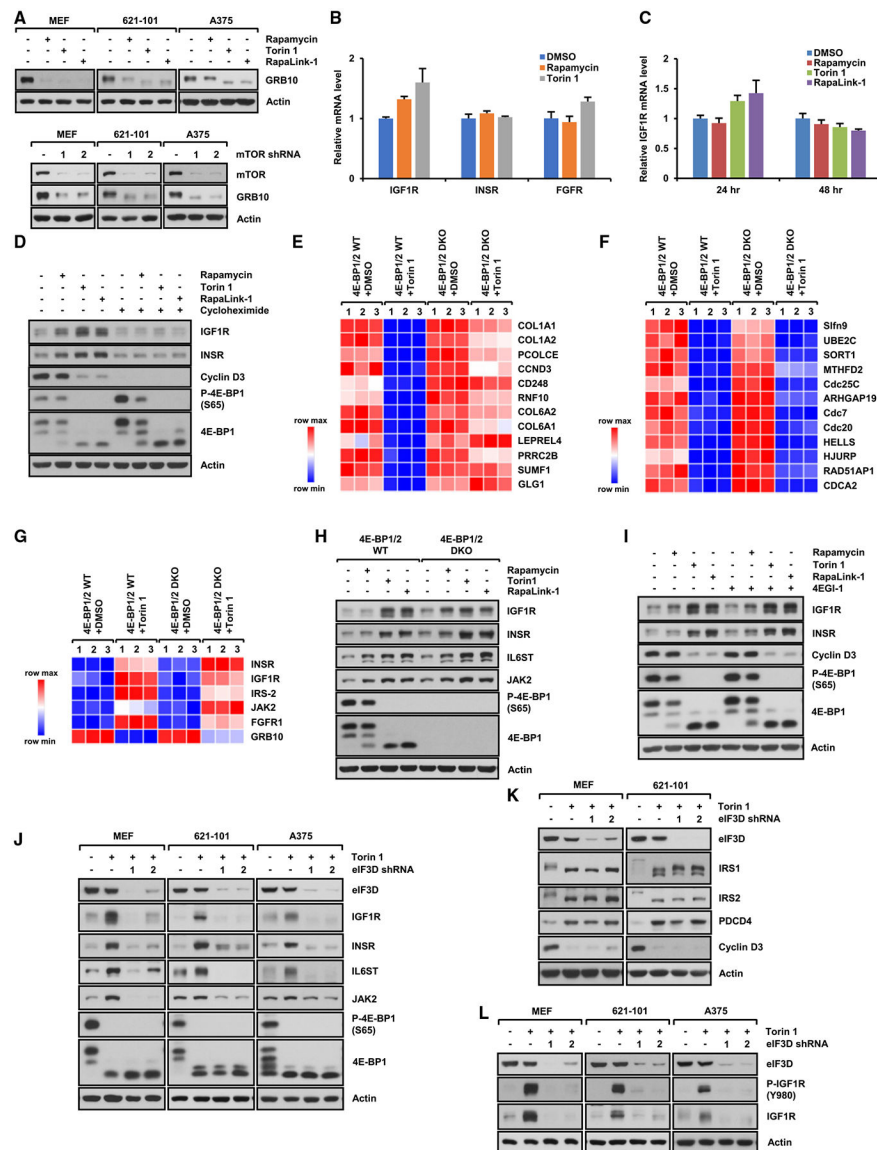
Figure 5. mTOR inhibition induces eIF3D-dependent mRNA translation

(A) Cells treated with/without rapamycin (20 ng/mL), Torin1 (250 nM), and RapaLink-1 (10 nM) for 24 h or stable mTOR knockdown cells were lysed, and immunoblot analysis was performed.

(B and C) MEFs were treated with mTOR inhibitors for (B and C) 24 h and (C) 48 h, and qRT-PCR was performed. Data are the mean ± SD of three technical replicates.

(D) MEFs were treated with cycloheximide (10 μg/mL) for 1 h, after which mTOR inhibitors were treated for an additional 23 h in the presence/absence of cycloheximide. Immunoblot analysis was performed.

(E–G) 4E-BP1/2 WT and DKO MEFs were treated with Torin1 for 24 h. Quantitative mass spectrometry for full protein profiling and data analysis were performed. The heatmaps show examples of (E) 4E-BP-dependent downregulation, (F) 4E-BP-independent downregulation, and (G) 4E-BP-independent upregulation of proteins following mTOR inhibition.

(H) 4E-BP1/2 WT and DKO MEFs were treated with mTOR inhibitors for 24 h, and immunoblot analysis was performed.

(I) MEFs were treated with 4EGI-1 (25 μM) for 1 h, after which mTOR inhibitors were treated for an additional 23 h in the presence/absence of 4EGI-1. Cells were lysed, and immunoblot analysis was performed.

(J–L) Stably knocked-down cells with eIF3D shRNAs were treated with Torin1 for 24 h, and immunoblot analysis was performed.

See also Figure S5.
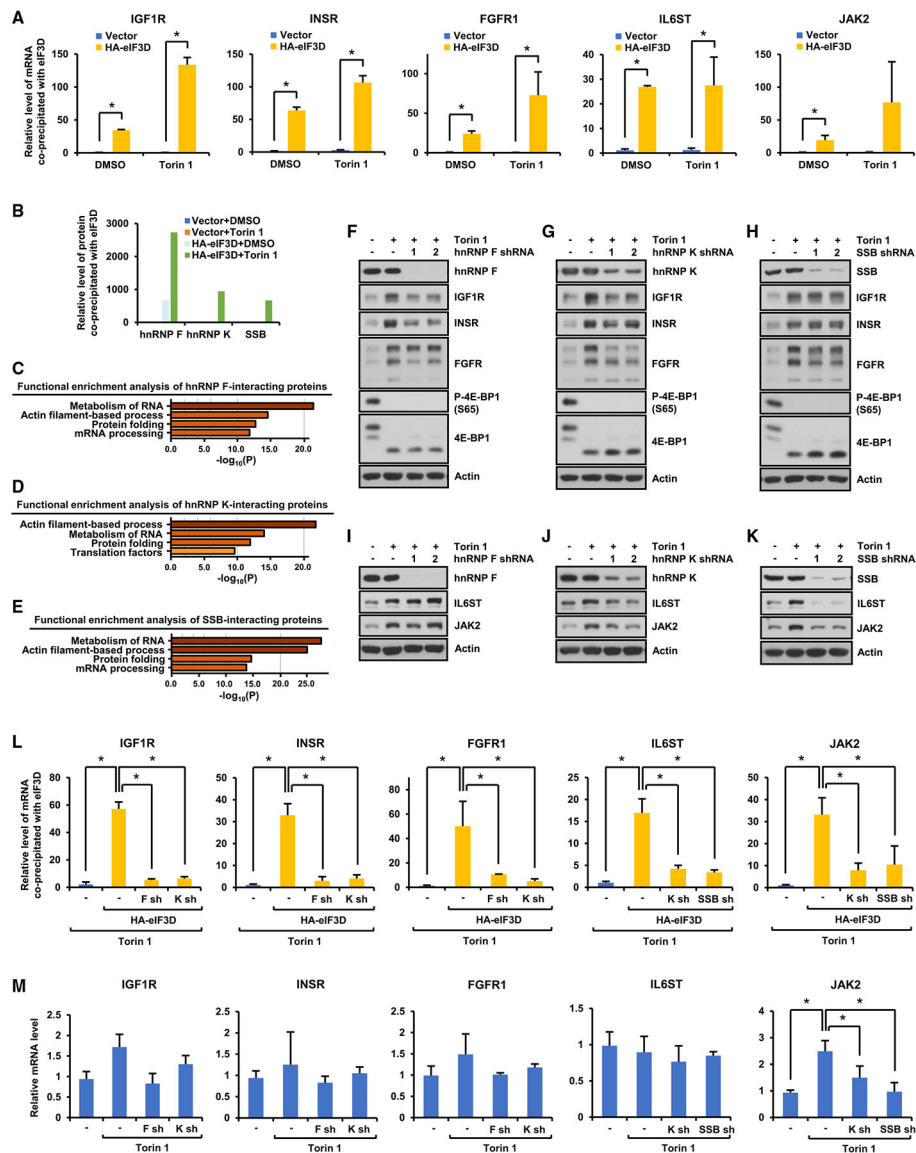
Figure 6. eIF3D and RBPs cooperate to regulate mRNA translation following mTOR inhibition

(A) MEFs stably expressing HA-eIF3D proteins were treated with/without Torin1 (250 nM) for 24 h, and RNA immunoprecipitation and qRT-PCR were performed. Data are the mean ± SD of three technical replicates. Statistical significance (*p < 0.05) was assessed by t test.

(B) eIF3D interacting RBPs identified by mass spectrometry.

(C–E) MEFs stably expressing control, HA-hnRNPF (C), HA-hnRNPK (D), and HA-SSB (E) were treated with Torin1 for 24 h, and their interacting proteins were identified and analyzed.

(F–K) Stably knocked down MEFs with indicated shRNAs were treated with/without Torin1 for 24 h, and immunoblot blot analysis was performed.

(L) RBP knockdown MEFs expressing HA-eIF3D were treated with Torin1 for 24 h, and RNA immunoprecipitation and qRT-PCR were performed. Data are the mean ± SD of three technical replicates. Statistical significance (*p < 0.05) was assessed by t test.

(M) Stably knocked-down MEFs with indicated shRNAs were treated with/without Torin1 for 24 h, and qRT-PCR was performed. Data are the mean ± SD of three technical replicates. Statistical significance (*p < 0.05) was assessed by t test.

See also Figure S6.

Figure 7. mTOR inhibition increases the migratory and invasive potential of cells

(A–D) Quantitative protein profiling was performed with stable control or eIF3D-knockdown MEFs treated with/without Torin1 (250 nM) for 24 h. The heatmaps show examples of (A) eIF3D-dependent upregulation or (B) eIF3D-independent upregulation of proteins following mTOR inhibition. The graphs show enrichment analysis of proteins upregulated in a (C) eIF3D-dependent or (D) eIF3D-independent manner following mTOR inhibition.

(E–J) A375 cells were grown with/without Torin1 or RapaLink-1 for 48 h, after which (E, G, and H) migration and (F, I, and J) invasion assays were performed as described in the STAR Methods. IGF1R inhibitors (BMS754807: 5 µM, OSI-906: 5 µM), IL-6ST inhibitor (SC144: 5 µM), and JAK1/2 inhibitors (ruxolitinib: 2.5 µM, momelotinib: 5 µM). Scale bars: 500 µm. Data are the mean ± SD of three biological replicates. Statistical significance (*p < 0.05) was assessed by t test.

KEY RESOURCES TABLE

REAGENT or RESOURCE	SOURCE	IDENTIFIER
Antibodies		
Anti-phospho-T308-Akt	Cell Signaling Technology	13038, RRID: AB_2629447
Anti-phospho-S473-Akt	Cell Signaling Technology	4060, RRID: AB_2315049
Anti-total Akt	Cell Signaling Technology	4691, RRID: AB_915783
Anti-phospho-S65-4E-BP1	Cell Signaling Technology	9451, RRID: AB_330947
Anti-4E-BP1	Cell Signaling Technology	9644, RRID: AB_2097841
Anti-4E-BP2	Cell Signaling Technology	2845, RRID: AB_10699019
Anti-phospho-T389-S6K1	Cell Signaling Technology	9234, RRID: AB_2269803
Anti-S6K1	Cell Signaling Technology	2708, RRID: AB_390722
Anti-phospho-S235/236-S6	Cell Signaling Technology	2211, RRID: AB_331679
Anti-S6	Cell Signaling Technology	2317, RRID: AB_2238583
Anti-phospho-Y980-IGF1R	Cell Signaling Technology	4568S, RRID: AB_2122279
Anti-IGF1R	Cell Signaling Technology	3018, RRID: AB_560943
Anti-phospho-S636/639-IRS1	Cell Signaling Technology	2388, RRID: AB_330339
Anti-IRS1	Cell Signaling Technology	2382, RRID: AB_330333
Anti-IRS2	Cell Signaling Technology	3407, RRID: AB_2127860
Anti-insulin receptor	Cell Signaling Technology	3025, RRID: AB_2280448
Anti-mTOR	Cell Signaling Technology	2983, RRID: AB_2105622
Anti-phospho-Y1007/1008-JAK2	Cell Signaling Technology	3771, RRID: AB_330403
Anti-JAK2	Cell Signaling Technology	3230, RRID: AB_2128522
Anti-phospho-Y705-STAT3	Cell Signaling Technology	9145, RRID: AB_2491009
Anti-Rictor	Cell Signaling Technology	2140, RRID: AB_2179961
Anti-PDCD4	Cell Signaling Technology	9535, RRID: AB_2162318
Anti-eIF4E	Cell Signaling Technology	9742, RRID: AB_823488
Anti-eIF4E2	Cell Signaling Technology	79940, RRID: AB_2936837
Anti-eIF4G	Cell Signaling Technology	2469, RRID: AB_2096028
Anti-eIF4G2	Cell Signaling Technology	5169, RRID: AB_10622189
Anti-cyclin D3	Cell Signaling Technology	2936, RRID: AB_2070801
Anti-FGFR	Cell Signaling Technology	9740, RRID: AB_11178519
Anti-La Antigen (SSB)	Cell Signaling Technology	5034, RRID: AB_10620954
Anti-phospho-S9-GSK3	Cell Signaling Technology	9323, RRID: AB_2115201
Anti-GSK3	Cell Signaling Technology	9315, RRID: AB_490890
Anti-GP130	Cell Signaling Technology	3732, RRID: AB_2125953
Anti-Grb10	Cell Signaling Technology	3702, RRID: AB_2112883
Anti-Grb10	Novus Biologicals	NBP2-41159, RRID:N/A
Anti-eIF3B	Novus Biologicals	NBP2-24571, RRID:N/A
Anti-hnRNPK	Proteintech	11426-1-AP, RRID: AB_2264314
Anti-hnRNPF	Proteintech	67701-1-IG, RRID: AB_2882893
Anti-STAT3	Proteintech	10253-2-AP, RRID: AB_2302876
Anti-phospho-Tyr612-IRS1	Millipore Sigma	09-432, RRID: AB_1163457

REAGENT or RESOURCE	SOURCE	IDENTIFIER
Anti-actin	Millipore Sigma	A5441, RRID: AB_476744
Anti-eIF3D	Santa Cruz Biotechnology	SC-271515, RRID: AB_10659103
Chemicals, peptides, and recombinant proteins		
Rapamycin	Selleckchem	S1039
Torin1	Selleckchem	S2827
Rapalink1	Dr. Kevan Shokat	N/A
Sapanisertib	Selleckchem	S2811
Erlotinib	Selleckchem	S1023
BMS754807	Selleckchem	S1124
Infigratinib	Selleckchem	S2183
Crenolanib	Selleckchem	S2730
Ruxolitinib	Selleckchem	S1378
Momelotinib	Selleckchem	S2219
C188-9	Selleckchem	S8605
OSI906	Selleckchem	S1091
4EGI-1	Selleckchem	S7369
Cycloheximide	Millipore Sigma	C4859
Critical commercial assays		
Click-IT AHA (L-Azidohomoalanine)	ThermoFisher Scientific	C10102
Tetramethylrhodamine (TAMRA) Alkyne	ThermoFisher Scientific	T10183
Click-iT Protein Reaction Buffer Kit	ThermoFisher Scientific	C10276
Deposited data		
Raw and processed data	This paper	GEO: GSE229623
Raw data	This paper	ProteomeXchange: PXD041933
Experimental models: Cell lines		
A375	ATCC	CRL-1619
621–101	Dr. Jane Yu	N/A
4E-BP1&2 WT and KO MEFs	Dr. Nahum Sonenberg	N/A
Rictor WT and KO MEFs	Dr. Brendan Manning	N/A
293T	Dr. Andrew L. Kung	N/A
Recombinant DNA		
pLKO.1-mTOR shRNAs	Millipore Sigma	SHCLNG-NM_004958
pLKO.1-mTOR shRNAs	Millipore Sigma	SHCLNG-NM_020009
pLKO.1-eIF3D shRNAs	Millipore Sigma	SHCLNG-NM_003753
pLKO.1-eIF3D shRNAs	Millipore Sigma	SHCLNG-NM_018749
pLKO.1-hnRNPF shRNAs	Millipore Sigma	SHCLNG-NM_133834
pLKO.1-hnRNPK shRNAs	Millipore Sigma	SHCLNG-NM_025279
pLKO.1-SSB shRNAs	Millipore Sigma	SHCLNG-NM_009278
Software and algorithms		
Metascape	Open source	https://metascape.org
GelQuantNet V1.8.2	Open source	http://biochemlabsolutions.com/GelQuantNET.html

REAGENT or RESOURCE	SOURCE	IDENTIFIER
GraphPad Prism 9	GraphPad Software, Inc.	RRID: SCR_002798
Excel	Microsoft	RRID: SCR_016137
BioRender	BioRender	RRID: SCR_018361
Other		
Mass Spectrometry	Dr. Noah Dephoure	N/A
Mass Spectrometry	Multiplexed Proteomics Center at Harvard Medical School	N/A